ACS OMEGA

http://pubs.acs.org/journal/acsodf

Article

Synthesis and Biological Evaluation of Coumarin Triazoles as Dual Inhibitors of Cholinesterases and β-Secretase

Ankita Sharma and Sandip B. Bharate*

Cite This: *ACS Omega* 2023, 8, 11161−11176

Read Online

ACCESS | Metrics & More | Article Recommendations | Supporting Information

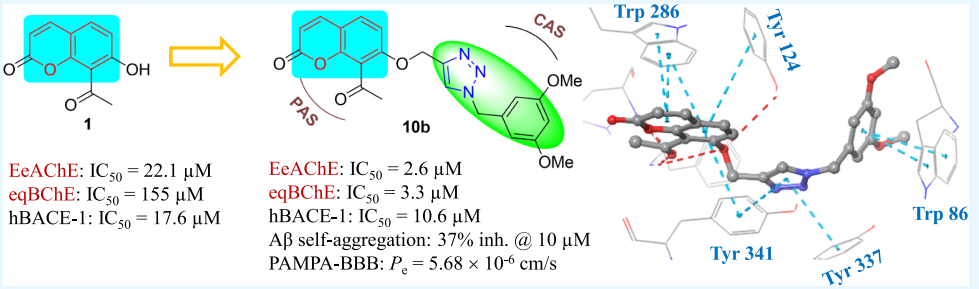

ABSTRACT: Coumarin is a naturally occurring bioactive pharmacophore with wide occurrence among central nervous system (CNS)-active small molecules. 8-Acetylcoumarin, one of the natural coumarins, is a mild inhibitor of cholinesterases and β-secretase, which are vital targets of Alzheimer's disease. Herein, we synthesized a series of coumarin−triazole hybrids as potential multitargeted drug ligands (MTDLs) with better activity profiles. The coumarin−triazole hybrids occupy the cholinesterase active site gorge from the peripheral to the catalytic anionic site. The most active analogue, **10b**, belonging to the 8-acetylcoumarin core, inhibits acetylcholinesterase (AChE), butyrylcholinesterase (BChE), and β-secretase-1 (BACE-1) with IC_{50} values of 2.57, 3.26, and 10.65 μM, respectively. The hybrid, **10b**, crosses the blood−brain barrier *via* passive diffusion and inhibits the self-aggregation of amyloid-β monomers. The molecular dynamic simulation study reveals the strong interaction of **10b** with three enzymes and forming stable complexes. Overall, the results warrant a detailed preclinical investigation of the coumarin−triazole hybrids.

1. INTRODUCTION

Alzheimer's disease (AD) is a multifaceted progressive neurodegenerative disease with a time lag between the onset of a responsible biochemical process and the first found symptom. The former begins to cause neuronal damage many years advance when the latter is found. The impaired cholinergic transmission, accumulation of amyloid-β (Aβ) plaques, and neurofibrillary tangles in the brain are major hallmarks of AD that gradually lead to the death of nerve cells and brain atrophy.[1] Hampering of the cholinergic transmission results in memory and attention-deficit issues. This hampering is caused due to overactivity of acetylcholinesterase (AChE), which causes the breakdown of the somatic neurotransmitter acetylcholine (ACh).[2] Donepezil and galantamine are selective Food and Drug Administration (FDA)-approved AChE inhibitors. In the normal brain, the loss of ACh is compensated by butyrylcholine (BCh), but in AD, the levels of BCh are also depleted due to overexpression of the butyrylcholinesterase (BChE).[3] This makes the dual inhibition of AChE and BChE important enzymatic targets. Rivastigmine is the only FDA-approved dual cholinesterase (ChE) inhibitor.[4]

The Aβ accumulation is considered a major culprit in AD pathology. The cleavage of Aβ precursor protein (APP) is responsible for forming the Aβ oligomers and plaques in the amyloidogenic pathway. In the nonamyloidogenic pathway, α-secretase cleaves the APP into water-soluble fragments, which could be eliminated from the body. In the amyloidogenic pathway, the cleavage of APP is caused by β-secretase (BACE-1 or Aβ precursor cleaving enzyme), which leads to the formation of insoluble waxy fragments called Aβs.[5] This makes BACE-1 a vital target in AD drug development. Besides, the amyloid β 1−42 ($Aβ_{1-42}$) is a self-aggregatory protein;[6] thus, inhibition of its spontaneous aggregation is also an important target.[7] The recently approved aducanumab is an anti-amyloid monoclonal antibody, the only disease-modifying therapy for treating AD. In contrast, all other marketed drugs only provide temporary relief but do not cure or alter the underlying pathogenesis of the disease.[8]

Natural products (NPs) have been the basis of traditional medicines throughout history. NPs are recognized to have chemical diversity and biochemical specificity, rendering them

Received: December 15, 2022
Accepted: March 6, 2023
Published: March 16, 2023

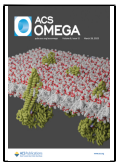

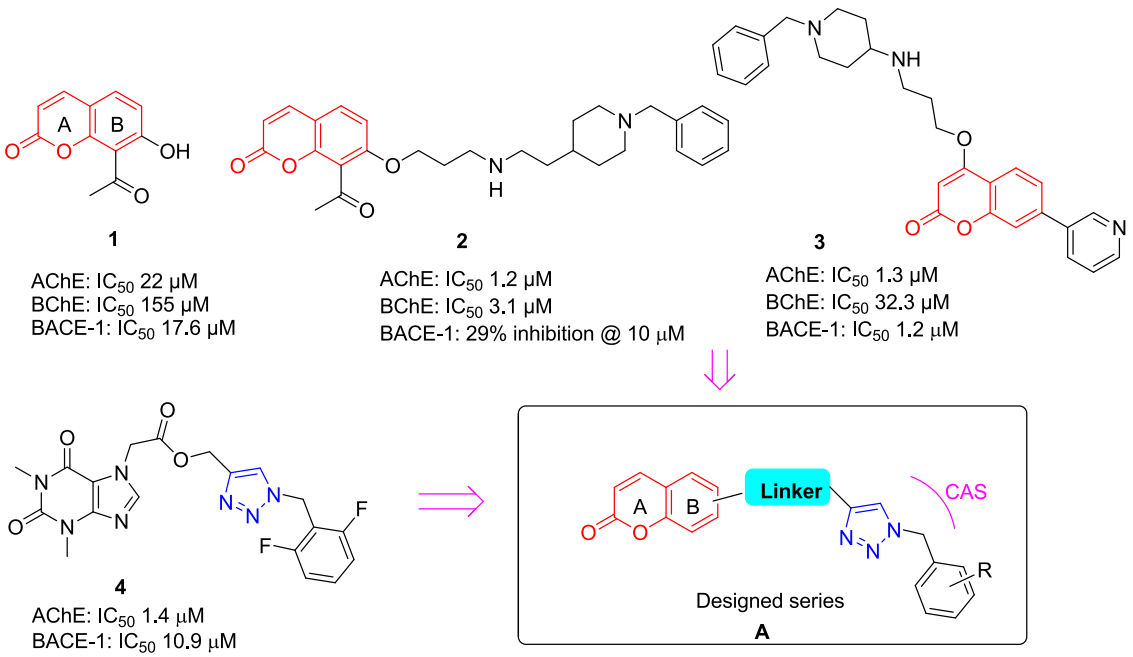

Figure 1. Chemical structures of coumarin derivatives **1**−**3** and triazole **4** that are reported to show dual ChE/BACE-1 inhibition. The proposed coumarin−triazole series is also shown with general structure **A**. Here, the coumarin may be connected to the triazole through ring A or B.

Scheme 1. Synthesis of Coumarin A-Ring Connected Triazole Hybrids, 8a−p[a]

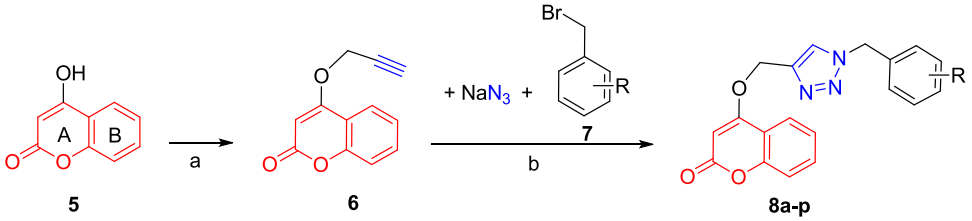

[a]Reagents and conditions: (a) propargyl bromide, K_2CO_3, dimethylformamide (DMF), 70 °C, 24 h, reflux, 95%; (b) TEA, sodium ascorbate, $CuSO_4{\cdot}5H_2O$, room temperature (rt), 24 h, 54−85%.

promising leads as such or *via* vital synthetic modifications in drug discovery. The literature reveals that nearly 84% of the FDA-approved drugs for treating central nervous system (CNS) diseases belong to NPs.[9] NPs with coumarin motifs have been extensively studied for drug discovery and development as it is a multitargeted ligand with minimal toxic side effects. Coumarins are the NPs containing benzopyrone nucleus, which occurs in over 1300 secondary metabolites from terrestrial and marine sources.[10] The conjugated double-bond system of coumarin has been interestingly manifested in medicinal chemistry and chemical biology. Many synthetic coumarins exhibit a broad spectrum of biological activities for treating various ailments like cancer,[11] infectious diseases,[12] diabetes,[13] and neurological disorders.[14] The FDA-approved coumarin class of drugs comprises anticoagulants such as warfarin, acenocoumarin, and the antibiotic novobiocin.[15] Coumarin pharmacophore has been documented with neuroprotective and anti-Alzheimer properties.[16] Thus, its relative availability, low toxicity, and ethnopharmacological importance have made it prudent to explore new derivatives of coumarins for AD.[17] The coumarin-based compounds show anti-cholinesterase activity. The 8-acetylcoumarin **1** is a moderate inhibitor of AChE and BACE-1. Its hybrid structure **2** with donepezil shows improvement in the AChE and BACE-1 inhibition activity.[18] Similarly, Zhao's group has recently reported another coumarin-donepezil hybrid, **3**, with dual ChE/BACE-1 inhibition activity.[19] In both these hybrid structures, incorporating benzyl-piperidine into the structure helps interact with the catalytic site of ChEs. Recently, we reported that the placement of benzyl triazole (*e.g.*, compound **4**) to the AChE pharmacophore also helps to gain the interaction at the catalytic site of ChEs.[20] Besides, the triazole-based compounds are known to show inhibition of ChEs,[21] BACE-1,[22] and Aβ-aggregation.[23] Thus, based on the literature precedence, we synthesized coumarin−triazole hybrids (general structure shown in Figure 1) as potential dual inhibitors of ChEs and BACE-1.

2. RESULTS AND DISCUSSION

2.1. Synthesis and *In Vitro* Biological Evaluation. The first series of coumarin−triazole hybrids were synthesized with 4-hydroxycoumarin (**5**) as a precursor. The propargylation of 4-hydroxycoumarin yielded 4-*O*-propargylated coumarin **6**. The click reaction of propargyl product with the benzyl bromide (**7a**) in the presence of sodium azide yielded the corresponding triazole, **8a**, in 82% yield, as shown in Scheme 1. Various substituted benzyl bromides (**7**) also participated in the click reaction to produce corresponding triazoles, **8b**−**p**, in good yields.

https://doi.org/10.1021/acsomega.2c07993
ACS Omega 2023, 8, 11161−11176

Table 1. Cholinesterase and BACE-1 Inhibition Results for Coumarin A-Ring Connected Triazole Hybrids, 8a−p

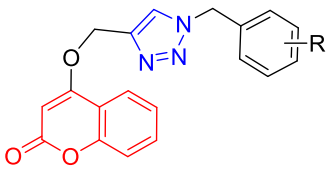

entry	R	IC_{50} (μM) ± SD		
		EeAChE	eqBChE	hBACE-1
5		138.56 ± 1.85	167.06 ± 5.63	168.63 ± 7.67
8a	H	150.70 ± 3.14	212.4 ± 2.55	72.90 ± 2.40
8b	2-Cl	68.71 ± 0.71	42.22 ± 0.78	186.6 ± 1.21
8c	3-Cl	62.64 ± 2.40	61.9 ± 3.66	24.82 ± 1.49
8d	2,6-Cl	59.41 ± 2.71	40.29 ± 0.93	105.83 ± 1.38
8e	2-F	89.23 ± 1.88	62.32 ± 1.20	111.23 ± 0.63
8f	3-F	232.76 ± 2.31	235.8 ± 3.60	22.32 ± 1.54
8g	4-F	193.6 ± 2.19	249.4 ± 3.1	24.22 ± 1.98
8h	2,6-F	73.89 ± 0.63	66.66 ± 1.37	134.53 ± 1.90
8i	2-CF_3	4.83 ± 0.11	7.04 ± 0.77	10.17 ± 0.79
8j	4-CF_3	23.26 ± 2.86	209.13 ± 2.11	19.54 ± 0.66
8k	2-OCF_3	9.13 ± 0.73	9.95 ± 0.89	17.98 ± 1.59
8l	4-OCF_3	45.39 ± 1.40	157.5 ± 1.98	132.9 ± 1.08
8m	2-CH_3	210.7 ± 1.83	171.6 ± 1.98	161.5 ± 1.85
8n	3-OCH_3	11.39 ± 1.16	139.7 ± 6.25	125.7 ± 4.18
8o	3,5-di-OCH_3	2.76 ± 0.04	3.30 ± 0.01	9.79 ± 1.36
8p	4-NO_2	200.4 ± 0.85	219.8 ± 3.04	156.03 ± 1.09
cryptolepine		0.33 ± 0.2	0.61 ± 0.3	nt[a]
donepezil		0.025 ± 0.005	5.72 ± 0.59	nt
β-secretase inhibitor IV		nt	nt	0.019 ± 0.006

[a]nt: not tested.

All prepared coumarin triazoles **8a−p** were screened for inhibition of ChEs and BACE-1 using the Ellman and fluorescence resonance energy transfer (FRET) assay, and results are summarized in Table 1. Cryptolepine and donepezil were used as positive controls for ChEs. Cryptolepine is a potent dual inhibitor of ChEs reported by us.[24] Donepezil is an FDA-approved ChE inhibitor. The commercially available β-Secretase inhibitor IV was used as a positive control for BACE-1.[25] The 4-hydroxycoumarin **5** is a poor inhibitor of AChE, BChE, and BACE-1. The condensation of **5** with the benzyl triazole did not significantly boost the inhibition of ChEs; however, a marginal improvement in BACE-1 inhibition was observed (**5** *vs* **8a**). However, placing various electron-withdrawing groups on the benzyl ring has helped dramatically increase the activity. The careful analysis of results provided structure−activity relationship (SAR) patterns. The boost in ChE inhibition by 2−3-fold was noticed simply by placing −Cl substitution on the benzyl ring (analogues, **8b**, **8c**, **8d**). The −F substitution also boosted ChE inhibition, but only at the ortho-position (analogue **8e**). The ortho-substitution with a powerful electron-withdrawing group, trifluoromethyl, yielded a compound **8i** that inhibits AChE, BChE, and BACE-1 with IC_{50} values of 4.83, 7.04, and 10.17 μM, respectively. Similarly, the *ortho*-OCF_3 substitution significantly boosted the inhibition of all three enzymes (analogue **8k**). However, the analogues with $-CF_3$ or $-OCF_3$ at para-position were less effective than ortho-substituted analogues. Methoxy substitution provided the best results with better activity, particularly by disubstituted analogues. The 3,5-dimethoxy-substituted analogue, **8o**, is the most active, with IC_{50} values of 2.76, 3.30, and 9.79 μM, respectively. Thus, it is clear that the substituents on the triazole benzyl ring play a vital role in the modulation of the activity of all three enzymes. The 2-trifluoromethyl-, 2-trifluoromethoxy-, 3-methoxy-, and 3,5-dimethoxy-substituted analogues were the most active in the coumarin A-ring connected triazole hybrid series.

Next, we synthesized a series of coumarin−triazole hybrids with triazole connected *via* the B-ring of coumarin. For this, we employed four different hydroxy coumarins, namely, 8-acetylcoumarin (**1**), 4-methyl-6,7-dihydroxycoumarin (**11**), 4-methyl-6-methoxy-7-hydroxycoumarin (**14**), and 7-hydroxy-coumarin (umbelliferone, **17**) as coumarin precursors. Based on the biological results of the **8a−p** series, 2-trifluoromethyl, 2-trifluoromethoxy, 3-methoxy, and 3,5-dimethoxybenzyl substitutions were used for synthesizing coumarin B-ring connected triazole hybrids. Using a similar synthetic strategy, four series of coumarin−triazole hybrids, **10a−d**, **13a−d**, **16a−d**, and **19a−d**, were synthesized as depicted in Scheme 2.

The biological screening results of coumarin B-ring-connected triazole hybrids are provided in Table 2. In the acetylcoumarin series, the hybrids with methoxy substitution were better than parent coumarin; however, trifluoromethyl and trifluoromethoxy substitutions were unfavorable as they resulted in the loss of activity against all three targets. The 4-methylcoumarin-based hybrids **13a−d** and **16a−d** were ineffective with all four benzylic substitutions. The unsubstituted coumarin-based hybrids, **19a−d**, were better inhibitors of ChEs than 4-methyl-substituted coumarin analogues. The 3-methoxybenzyl-containing coumarin−triazole **19a** displayed significant inhibition of ChEs with IC_{50} values of 3.6 and 2.8 μM, respectively. However, its dimethoxy analogue **19b** was not equally effective. Overall, the 3,5-dimethoxy analogue **10b**

https://doi.org/10.1021/acsomega.2c07993
ACS Omega 2023, 8, 11161−11176

Scheme 2. Synthesis of Coumarin B-Ring Connected Triazole Hybrids, 10a−d, 13a−d, 16a−d, and 19a−d[a]

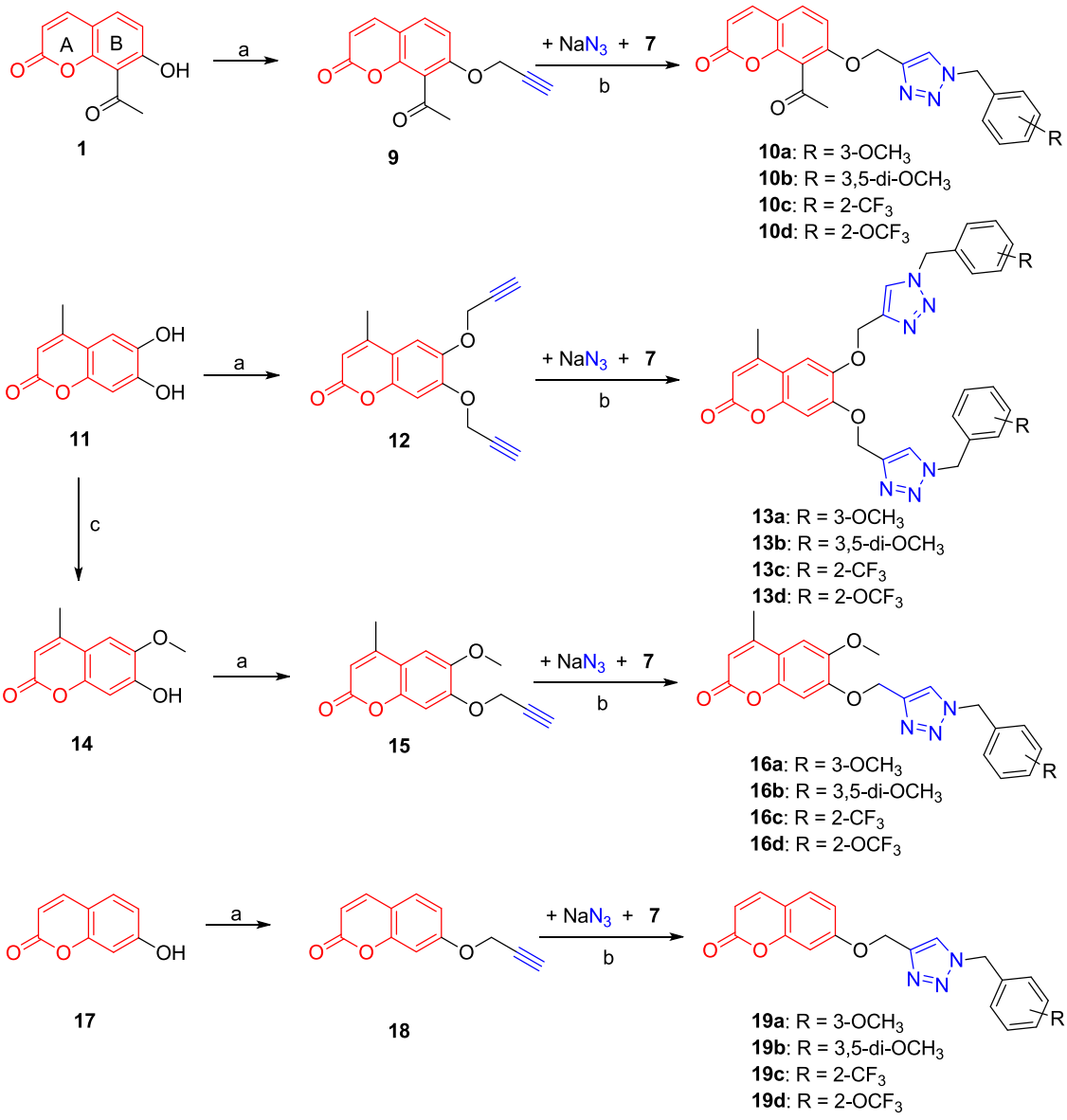

[a]Reagents and conditions: (a) propargyl bromide, K_2CO_3, DMF, 70 °C, 24 h, reflux, 75−91%; (b) TEA, NaN_3, sodium ascorbate, $CuSO_4{\cdot}5H_2O$, rt, 24 h, 50−80%; (c) methyl iodide, NaH, DMF, 0 °C, 90%.

from the acetylcoumarin series has potent inhibition of AChE and BChE and also BACE-1. However, the corresponding 3,5-dimethoxy analogues from other series, **13b**, **16b**, and **19b**, were not active to the level of **10b**. This probably indicates some role of the C8-acetyl group in the activity. Interestingly, compound **13b** is a selective BChE inhibitor with IC_{50} of 4.7 μM and shows poor activity against AChE and BACE-1. The dimethoxy substitution with the bis-triazole unit in **13b** probably fits appropriately in a wider BChE active site gorge but not in AChE active site gorge, which is comparatively narrower.

2.2. Enzyme Kinetics and Molecular Modeling for 10b. The enzyme kinetics of **10b** was carried out to assess the mode of inhibition for all three targets. The Lineweaver−Burk (LB) double-reciprocal plot for AChE indicates a non-competitive mode of inhibition with a k_i value of 0.27 μM (Figure 2A). However, for BChE and BACE-1, the depicted mode of inhibition is a mixed type with k_i values of 3.5 and 7 μM, respectively (Figure 2C,E). Further, we studied the interaction pattern of **10b** with each enzyme *via* molecular modeling studies. As depicted in Figure 2B, **10b** interacts with peripheral anionic site (PAS) as well as catalytic anionic site (CAS) residues of AChE. The acetylcoumarin core stays at the entrance of the gorge, and benzyl triazole orients toward the bottom of the cavity. Both the rings of coumarin form $\pi-\pi$ stacking with Trp 286 residue. Interestingly, the carbonyl oxygen of the acetyl group forms H-bonding with Arg 296 and Phe 296 residues, which could be the crucial factor for the superior activity of the acetylcoumarin series *vs* other series. The linker oxygen also forms H-bond with the Phe 295 residue. The triazole ring and aryl of coumarin form $\pi-\pi$ stacking with the Tyr 341 residue. The benzyl ring forms a vital $\pi-\pi$ stacking with Trp 86 residue of the anionic subsite of the CAS. The noncompetitive mode of inhibition, as seen in the kinetic study, could be because of the strong interaction of the **10b** with PAS residues *via* multiple $\pi-\pi$ stacking and H-bonds.

https://doi.org/10.1021/acsomega.2c07993
ACS Omega 2023, 8, 11161−11176

Table 2. Cholinesterase and BACE-1 Inhibition Results for Coumarin B-Ring Connected Triazole Hybrids, 10a−d, 13a−d, 16a−d, and 19a−d

		IC_{50} (μM) ± SD		
entry	R	EeAChE	eqBChE	hBACE-1
1		23.71 ± 3.21	155.03 ± 3.09	18.42 ± 1.04
11		68.14 ± 4.05	147.70 ± 5.46	104.8 ± 3.48
14		89.09 ± 3.51	146.07 ± 4.91	91.09 ± 2.41
17		164.46 ± 5.22	180.33 ± 4.58	174.53 ± 4.37
10a	3-OCH_3	8.36 ± 1.29	7.40 ± 0.94	118.8 ± 2.49
10b	3,5-di-OCH_3	2.57 ± 0.31	3.26 ± 0.13	10.65 ± 0.47
10c	2-CF_3	173.06 ± 1.89	44.60 ± 1.84	138.8 ± 1.47
10d	2-OCF_3	139.20 ± 1.64	170.10 ± 1.76	141.9 ± 1.59
13a	3-OCH_3	130.70 ± 0.45	51.70 ± 1.42	128.6 ± 1.49
13b	3,5-di-OCH_3	167.53 ± 6.70	4.7 ± 0.67	115.2 ± 3.86
13c	2-CF_3	154.70 ± 1.42	82.54 ± 1.41	139.4 ± 1.00
13d	2-OCF_3	176.0 ± 10.25	167.06 ± 5.63	20.72 ± 0.93
16a	3-OCH_3	164.2 ± 1.84	95.82 ± 1.12	138.4 ± 1.02
16b	3,5-di-OCH_3	150.96 ± 5.05	191.2 ± 1.13	9.06 ± 0.88
16c	2-CF_3	141.7 ± 0.89	57.45 ± 1.42	156.1 ± 1.42
16d	2-OCF_3	166.5 ± 2.45	141.03 ± 0.60	167.6 ± 1.40
19a	3-OCH_3	3.62 ± 0.33	2.80 ± 0.22	125.6 ± 3.92
19b	3,5-di-OCH_3	59.67 ± 0.62	63.24 ± 2.44	132.0 ± 2.02
19c	2-CF_3	20.64 ± 0.95	77.33 ± 6.38	17.71 ± 0.65
19d	2-OCF_3	52.54 ± 0.40	97.23 ± 1.29	172.8 ± 0.66
cryptolepine		0.33 ± 0.2	0.61 ± 0.3	nt[a]
donepezil		0.025 ± 0.005	5.72 ± 0.59	nt
β-secretase inhibitor IV		nt	nt	0.019 ± 0.006

[a]nt, not tested.

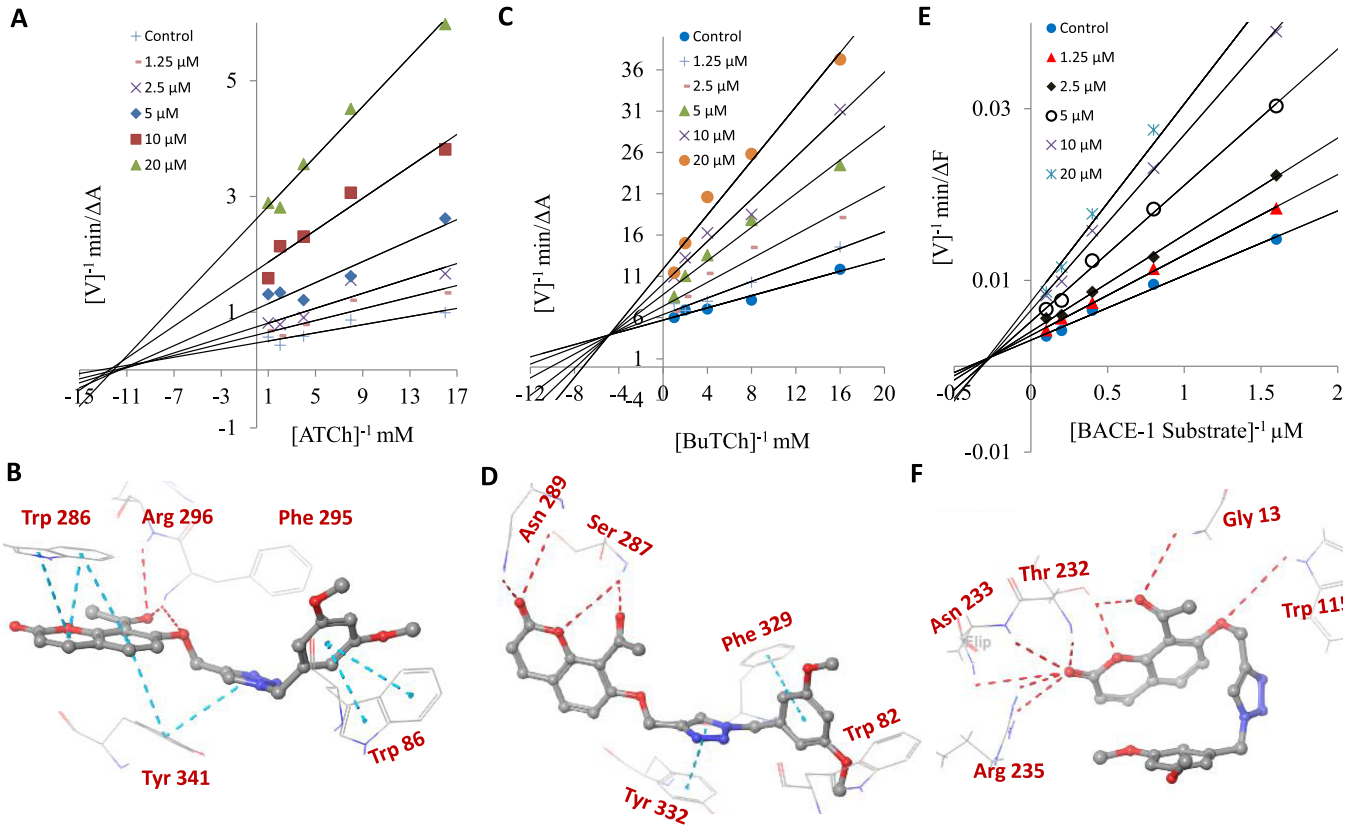

Figure 2. Enzyme kinetics and molecular modeling studies of **10b** with AChE, BChE, and BACE-1. (A) LB plot for inhibition of AChE by **10b**; (B) molecular docking of **10b** with AChE (PDB: 4EY7); (C) LB plot for inhibition of BChE by **10b**; (D) molecular docking of **10b** with BChE (PDB: 6EP4); (E) LB plot for inhibition of BACE-1 by **10b**; (F) molecular docking of **10b** with the BACE-1 (PDB: 1W51). The light blue dotted lines indicate $\pi-\pi$ interactions, and the dark red dotted lines indicate H-bonding interactions.

https://doi.org/10.1021/acsomega.2c07993
ACS Omega 2023, 8, 11161−11176

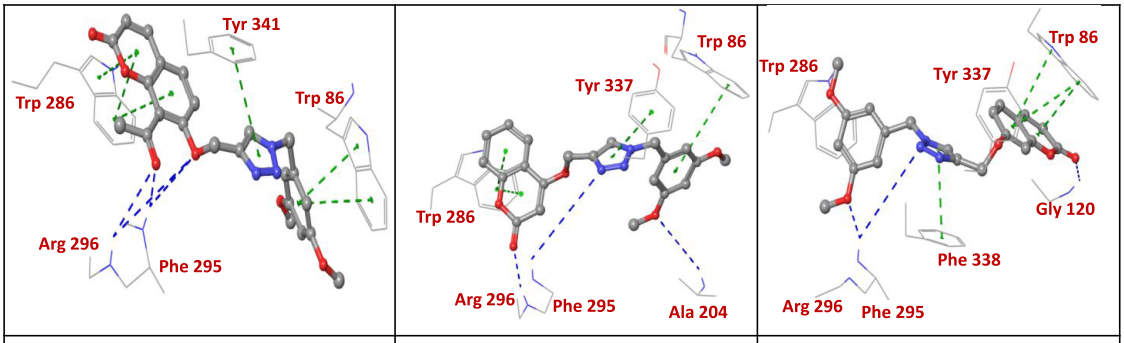

10b	8o	19b
Dock Score: −11.67 kcal/mol	Dock Score: −11.23 kcal/mol	Dock Score: −9.44 kcal/mol
EeAChE: IC_{50} = 2.6 μM	EeAChE: IC_{50} = 2.8 μM	EeAChE: IC_{50} = 59.7 μM

Figure 3. Interaction pattern of 3,5-dimethoxybenzyl coumarin−triazole hybrids, **10b**, **8o**, and **19b** with AChE (PDB: 4EY7).

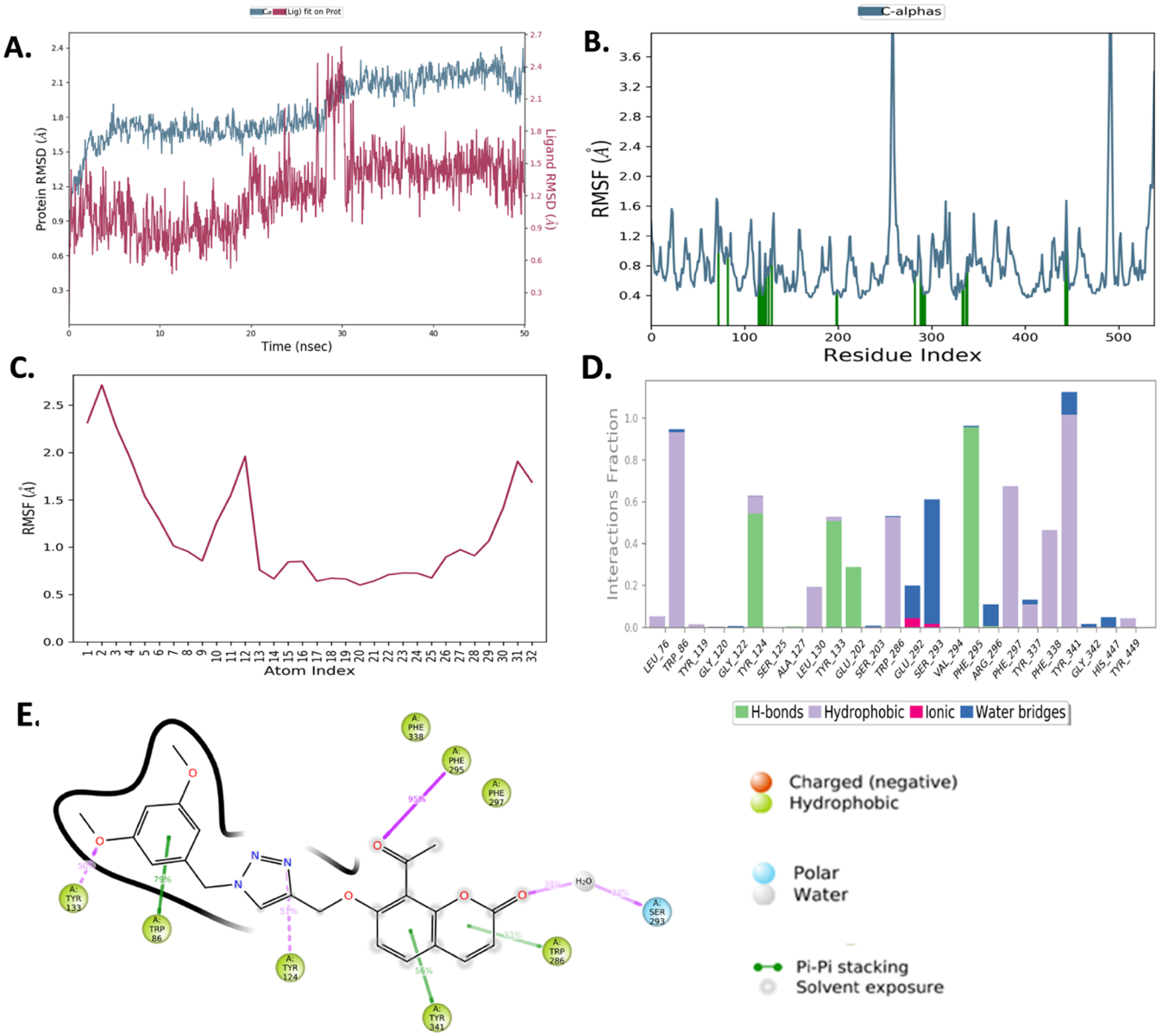

Figure 4. MD simulation of **10b**−AChE complex for 50 ns. (A) Protein−ligand RMSD during simulation; (B) RMSF of AChE; (C) RMSF of compound **10b**; (D) interaction pattern of compound **10b** with AChE during MD simulation; (E) two-dimensional (2D) diagram for the interaction of compound **10b** with AChE.

https://doi.org/10.1021/acsomega.2c07993
ACS Omega 2023, 8, 11161−11176

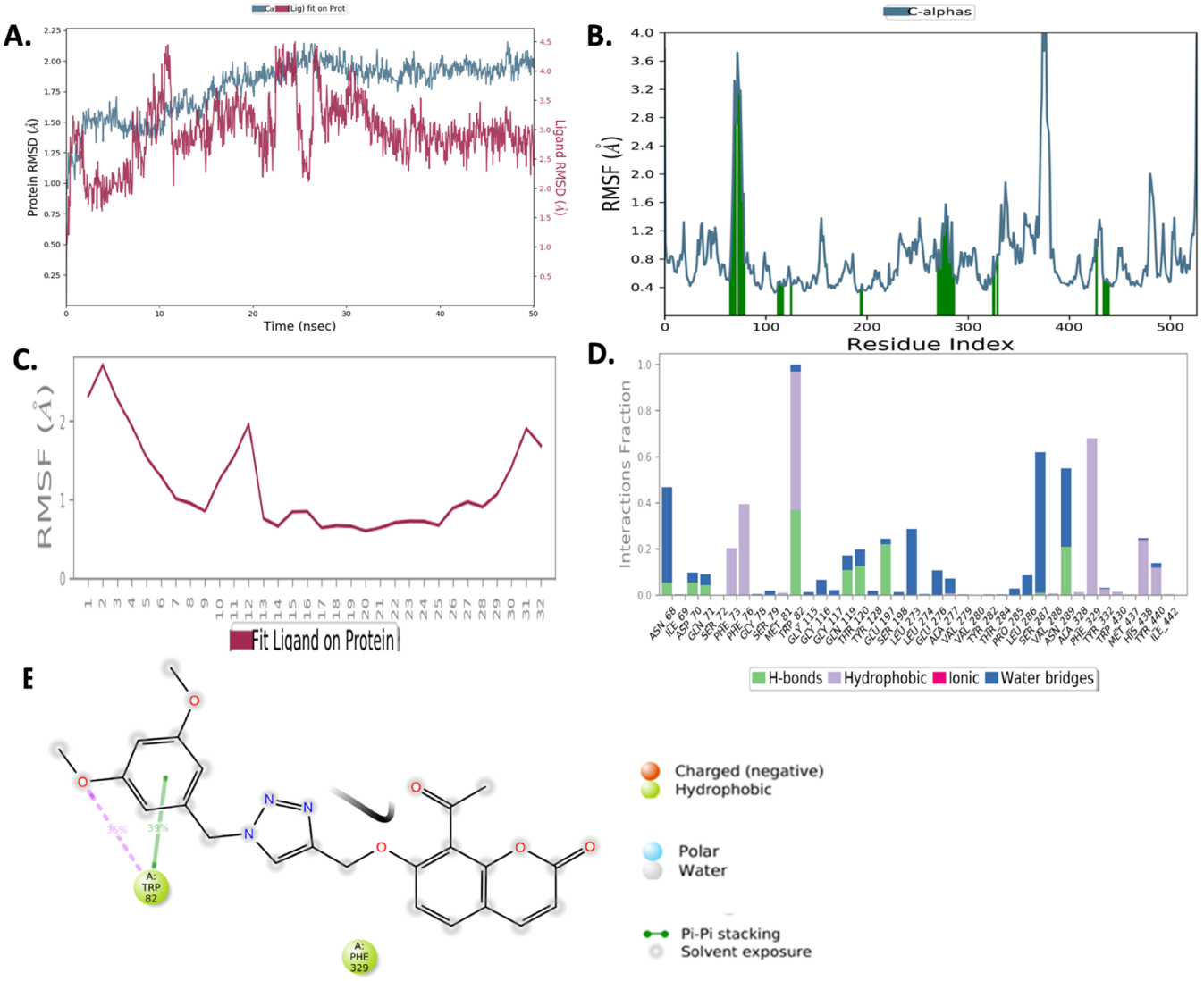

Figure 5. MD simulation of **10b**−BChE complex for 50 ns. (A) Protein−ligand RMSD during simulation; (B) RMSF of BChE; (C) RMSF of compound **10b**; (D) interaction pattern of compound **10b** with BChE during MD simulation; (E) 2D diagram for compound **10b** interactions with BChE.

The docking study of **10b** with BChE (Figure 2D) shows $\pi-\pi$ interactions of benzyl with Phe 329 but not with the Trp 82 of the anionic subsite. The triazole ring forms $\pi-\pi$ stacking with Tyr 332. Like in the case of AChE, the acetyl group participated in vital H-bonding with the PAS residues of BChE. The carbonyl oxygen of acetyl forms H-bond with Ser 287, which is also H-bonded with a coumarin ring oxygen atom. Figure 2F shows the interactions of **10b** with BACE-1 (PDB: 1W51). It shows H-bonding with Thr 232, Asn 233, Arg 235, Gly 13, and Trp 115 residues; however, the interaction with Asp 32 and Asp 228 was missing. The interaction with these aspartate residues is vital for the potent inhibition of BACE-1.[26] This could be the reason for its low activity level against the BACE-1 enzyme.

To understand the superiority of 8-acetyl-7-hydroxycoumarin framework *vs* 4-hydroxycoumarin and 7-hydroxycoumarin, we analyzed the binding pattern of **10b**, **8o**, and **19b** in the AChE active site (Figure 3). These three analogues differ only *via* the coumarin framework; thus, their different activity is related to the coumarin−triazole linkage and substitution on coumarins. Both rings of coumarin core in **10b** and **8o** offered $\pi-\pi$ stacking with Trp 286 at PAS, whereas in **19b**, this $\pi-\pi$ interaction is missing. Molecule **19b** is flipped by 180° in the AChE active site, with the coumarin core oriented toward the bottom of the AChE active site gorge. The 3,5-dimethoxybenzyl unit of **19b** did not show $\pi-\pi$ stacking with Trp 286 though it offered H-bonding with Phe 295 residue. In particular, the bidentate H-bonding offered by acetyl carbonyl oxygen of **10b** with Phe 295 and Arg 296 was missing in **19b**, which could also be accounting for the 20-fold difference in AChE inhibition activity of **10b** *vs* **19b**.

The 50 ns molecular dynamic simulation was carried out for enzyme−inhibitor complexes to determine the stability. The complex of compound **10b** with AChE is stable throughout the study, as indicated by the root mean square deviation (RMSD) value below 3 Å for both protein and ligand (Figure 4A). The root mean square fluctuation (RMSF) plot shown in Figure 4B,C further indicates minimal fluctuations in the residues of protein and atom of the ligand (RMSF is below 4 Å) during the entire period of study. The orientation map of compound **10b** is depicted in Figure 4D,E. The hydrophobic interaction with Tyr 341 was sustained for >56% and Trp 86 for more

https://doi.org/10.1021/acsomega.2c07993
ACS Omega 2023, 8, 11161−11176

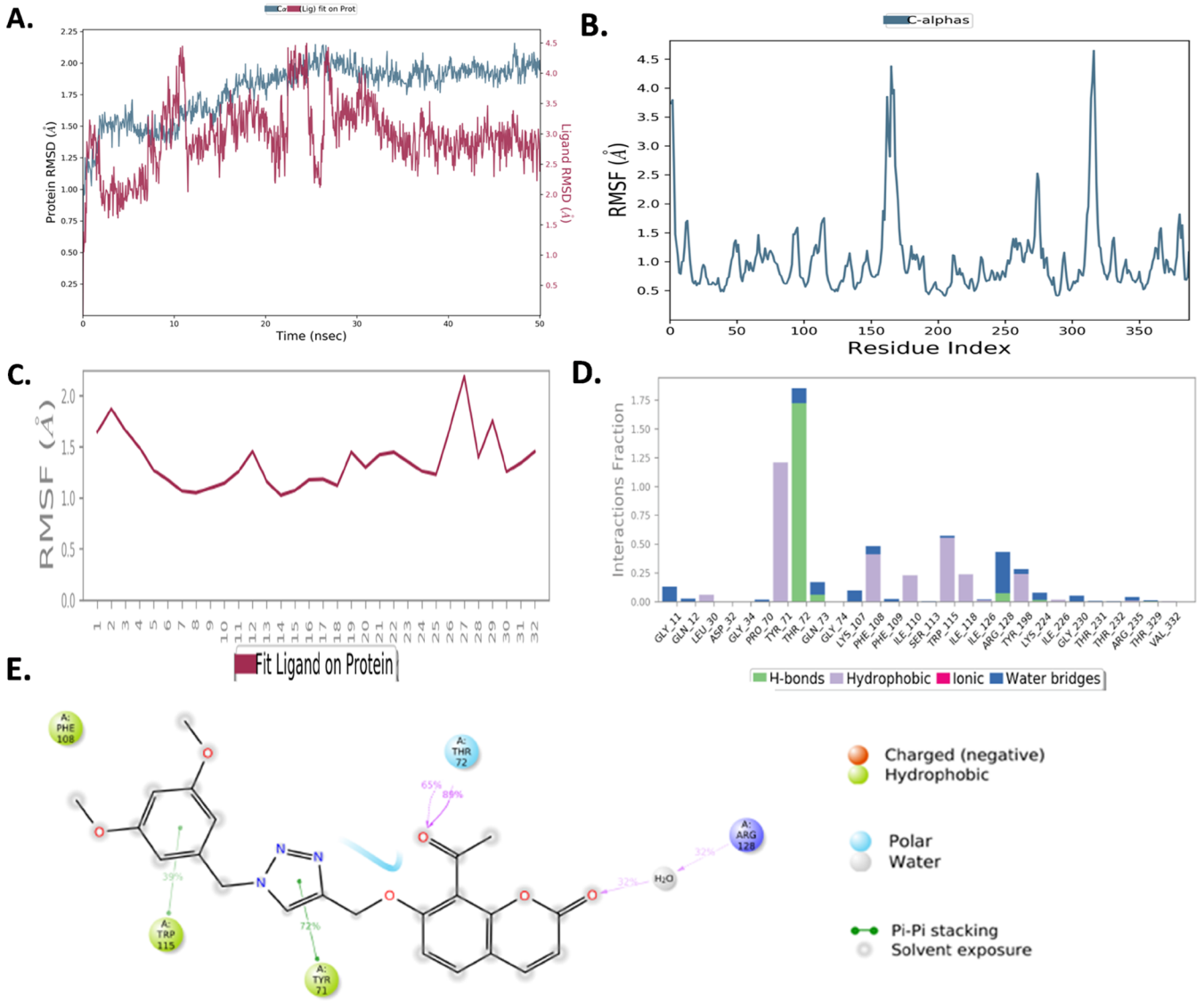

Figure 6. MD simulation of **10b**−BACE-1 complex for 50 ns. (A) Protein−ligand RMSD during simulation; (B) RMSF of BACE-1; (C) RMSF of compound **10b**; (D) interaction pattern of compound **10b** with BACE-1 during MD simulation; (E) 2D diagram for compound **10b** interactions with BACE-1.

than 79% of the simulation time. Tyr 124 shows H-bonding with the triazole ring for >51% of the simulation run. Trp 286 offers hydrophobic interactions for >33% of the simulation run. Phe 295 depicts H-bonding >95% persistently throughout the simulation study (Figure 4D,E).

As depicted in Figure 5A, the RMSD below 3 Å indicates the stability of the protein in the **10b**−BChE complex throughout the study. The ligand slightly diffuses from the initial binding site; however, the overall orientation and interaction pattern is unaffected (Figure 5A). The RMSF depicts a value below the range of 4 Å, which indicates no significant conformational changes along the protein chain as the ligand fits in the protein (Figure 5B,C). The most preserved interactions during the simulation run were hydrophobic $\pi-\pi$ stacking and H-bonding with Trp 82 for 39 and 36% of the run (Figure 5E).

The MD simulation of the **10b**−BACE-1 complex also indicated the stability of the complex. The RMSD for the protein is below 3 Å, which indicates stability. In contrast, for the ligand, RMSD is slightly above 3 Å, which is conclusive that the ligand diffuses away from the protein (Figure 6A). The RMSF for the protein and the ligand fit is below 3.5 and 2 Å, respectively (Figure 6B,C). The H-bonding between the acetyl group of coumarin with Thr 72 is sustained for >89% of the simulation time. The triazole ring also maintained hydrophobic interaction with the Tyr 71 residue for >72% of the simulation run. The hydrophobic interaction with Trp 115 residue is also retained for a significant time (Figure 6D,E).

2.3. Inhibition and Aβ Self-Aggregation. AD's main hallmark is forming Aβ plaques, which occur *via* the aggregation of Aβ monomers.[27] Thus, we evaluated the effect of compound **10b** on the self-aggregation of $A\beta_{1-42}$ monomers, which is one way to form oligomers and plaques. Analogue **10b** displayed a 37% inhibition of self-aggregation of $A\beta_{1-42}$ monomers, whereas the positive control, curcumin, showed 81% inhibition at 10 μM. The molecular docking of **10b** with the Aβ-monomer revealed that this compound binds to the metal binding site residue His 14; however, it does not interact with the Asp 23, the key residue in forming a salt bridge between monomers during the aggregation process.[28]

https://doi.org/10.1021/acsomega.2c07993
ACS Omega 2023, 8, 11161−11176

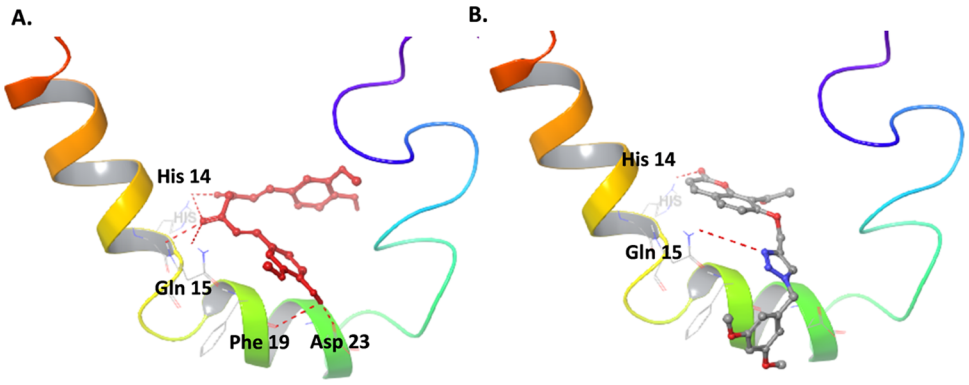

Figure 7. Molecular docking of curcumin (A) and compound **10b** (B) with the Aβ monomer (PDB: 1Z0Q).

Curcumin forms H-bonding with the metal binding site and the salt-bridge forming residue (Figure 7).

2.4. Parallel Artificial Membrane Permeability Assay (PAMPA)−Blood−Brain Permeability (BBB) Permeability and *In Silico* Absorption Distribution Metabolism Elimination (ADME) Properties of 10b. Along with the activity profile of the compound against various targets, CNS blood−brain permeability (BBB) is also an indispensable factor for a drug with CNS disease on target. The blood−brain barrier restricts molecules' passage from the brain vasculature to the brain due to its high trans-endothelial electrical resistance and low paracellular and transcellular permeability. Thus, the BBB permeability of **10b** was experimentally determined using a PAMPA assay (Table 3).

Table 3. BBB Permeability of 10b Determined Using PAMPA−BBB Assay

compound	λ_{max} (nm)	$P_e \times 10^{-6}$ cm/s ± SD	prediction of CNS permeation
10b	261	5.68 ± 1.1	CNS+
donepezil	270	13.32 ± 1.82	CNS+
theophylline	272	1.22 ± 1.38	CNS−

The ADME properties determine whether a compound has druglike properties. It is included at a very early stage of drug discovery. QikProp module of the Schrodinger molecular modeling software computationally determines the number of descriptors for small molecules, predicting the ADME properties.[29] These properties include total solvent-accessible surface area (SASA), the hydrophobic component of the SASA (FOSA), the hydrophilic component of the SASA (FISA), and the estimated number of H-bond donors (donorHB) and acceptors (accptHB) in aqueous solution. Table 4 also shows that the predicted ranges for the calculated partition coefficients, which are octanol/water (QP log $P_{o/w}$), aqueous solubility (QP log S), and skin permeability (QP log Kp) fall within the acceptable range. The computed IC_{50} for blockage of HERG K+ channels (QP log HERG), Caco-2 permeability, and Madin−Darby canine kidney (MDCK) permeability values are also within the normal limits. The BBB is also predicted computationally. The results show that QPlog BB also falls within the recommended range. This complies with the experimental results of the PAMPA assay, as shown in Table 3. ADME properties were also estimated for donepezil and β-secretase inhibitor IV and are listed in Table 4.

Table 4. ADME Properties for 10b and Positive Controls[a]

property	reference range	10b	donepezil	β-secretase inhibitor IV
molecular weight	300−1000	435.435	379.498	578.725
SASA	0−750	734.966	726.298	860.774
FOSA	7−330	324.954	410.311	391.518
FISA	0−6	139.219	58.288	123.351
donorHB	2−20	0	0	4
accptHB	2−20	9.25	5.5	12.7
QP log $P_{o/w}$	−2 to 6.5	2.77	4.436	3.543
QP log S	−6.5 to 0.5	−3.99	−4.904	−4.698
QP log HERG	concern below—5	−6.178	−6.868	−7.634
QPPCaco	<25 poor, >500 great	473.899	691.924	167.134
QP log BB	−3.0 to 1.2	−1.396	−0.021	−1.597
QPP MDCK	<25 poor, >500 great	220.701	367.58	40

[a]ADME properties were determined using the QikProp module of Schrodinger 10.2 software. Properties: total solvent-accessible surface area (SASA), the hydrophobic component of the SASA (FOSA), the hydrophilic component of the SASA (FISA), the estimated number of hydrogen-bond donor (donorHB) acceptor (accptHB) in aqueous solution. Also, QP log $P_{o/w}$ is the octanol/water partition coefficient, QP log S is aqueous solubility (mol/L), QP log HERG is IC_{50} value for blockage of HERG K^+ channels, QPPCaco is Caco-2 permeability (nm/s), QP log BB is brain/blood partition coefficient, and QPPMDCK is apparent MDCK cell permeability (nm/s). MDCK cells are considered a good mimic for the blood−brain barrier.

3. CONCLUSIONS

We designed and synthesized coumarin−triazole hybrid **10b**, displaying a multitargeted effect against AD targets, AChE, BChE, BACE-1, and Aβ-aggregation. It is predicted to cross the BBB based on the experimental PAMPA results and *in silico* QikProp prediction. The structure−activity relationship has been established for this scaffold, indicating that 3,5-dimethoxy substitution on the benzyl group along with the coumarin core with acetyl substitution is important for activity. The study also further validated the capability of triazole to interact at the CAS of the ChEs. The results presented herein warrant further investigation of **10b** in preclinical studies.

4. EXPERIMENTAL SECTION

4.1. General. The local suppliers of Sigma-Aldrich, TCI chemicals, and CDH have provided the chemicals, solvents, reagents, and the required glassware and plasticware for the

https://doi.org/10.1021/acsomega.2c07993
ACS Omega 2023, 8, 11161−11176

study. The enzymes, substrates, and positive controls for the biological studies are also procured from them. NMR spectra were recorded on a Bruker-Avance DPX FT-NMR 400 MHz instrument. IR spectra were recorded on a PerkinElmer IR spectrophotometer. High-resolution electrospray ionization mass spectra (HR-ESIMS) were obtained from an Agilent HR-ESIMS-6540-UHD machine. Absorbance and fluorescence readings were recorded on Molecular Devices and Biotage microplate readers, respectively. The absorbance readings in Ellman and PAMPA assays were recorded on SpectraMax Plus 384 plate reader. The fluorescence for the FRET assay was recorded on the Synergy H1 Hybrid Reader (Biotek). Melting points were recorded on a Buchi digital melting point apparatus.

4.2. Synthesis of 7-Hydroxy-6-methoxy-4-methyl-2*H*-chromen-2-one (14).[30] The mixture of compound **11** (0.52 mmol) and NaH (1.05 mmol) in 2 mL of DMF was stirred at 0 °C for half an hour. After half an hour, methyl iodide (0.52 mmol) was added, and the reaction was further stirred for 5 h at rt. After 5 h, the reaction mixture was added to 50 mL of ice-cold water to remove DMF efficiently. Extraction was done with EtOAc (3 × 50 mL). The EtOAc layer was concentrated on the vacuum evaporator to obtain **14** (1.2 g, yield: 90%). Brown powder; m.p. 130−131 °C; IR ($CHCl_3$) ν_{max} (cm^{-1}): 1710 (C═O), 1423 (C−O); ^{1}H NMR (400 MHz, $CDCl_3$): δ (ppm) 7.09 (s, 1H), 6.83 (s, 1H), 6.17 (s, 1H), 3.97 (s, 3H), 2.36 (s, 3H); ^{13}C NMR (100 MHz, $CDCl_3$): δ (ppm) 162.90, 153.90, 151.29, 150.02, 143.95, 114.82, 114.03, 109.71, 100.82, 57.82, 20.22; ESIMS: m/z 207.1 $[M + H]^+$; HR-ESIMS: m/z 207.0667 $[M + H]^+$ calcd for $C_{11}H_{10}O_4 + H^+$ (207.0657).

4.3. Propargylation of Coumarin Hydroxyl Group: Synthesis of 6, 9, 12, 15, and 18. The coumarin **1**, **5**, **11**, **14**, or **17** (1 equiv) was treated with potassium carbonate (4 equiv) in DMF for 30 min at 70 °C. After 30 min, propargyl bromide (1.5 equiv) was added, and the reaction was continued for 24 h. After 24 h, the reaction was cooled and poured into ice-cold water to remove the DMF. The extraction was done with EtOAc (3 × 50 mL). The combined ethyl acetate layer was concentrated on a rotary evaporator, and the residue was purified over silica gel (solvent system: 40% EtOAc in hexane) to obtain respective propargylated compounds, **6**, **9**, **12**, **15**, and **18**.

*4.3.1. 4-(Prop-2-yn-1-yloxy)-2H-chromen-2-one (**6**).*[31] White fluffy powder; yield, 95%; m.p.153−154 °C; IR ($CHCl_3$) ν_{max} (cm^{-1}): 1719 (C═O), 1251 (C−O); ^{1}H NMR (400 MHz, $CDCl_3$): δ (ppm) 7.85 (dd, J = 7.9, 1.5 Hz, 1H), 7.59−7.55 (m, 1H), 7.34−7.31 (m, 1H), 7.29 (d, J = 7.3 Hz, 1H), 5.84 (s, 1H), 4.88 (d, J = 16 Hz, 2H), 2.69 (t, J = 2.4 Hz, 1H); ^{13}C NMR (100 MHz, $CDCl_3$): δ (ppm) 164.29, 162.66, 153.52, 132.61, 125.004, 123.27, 116.69, 91.72, 78.20, 75.58, 56.87; ESIMS: m/z 201 $[M + H]^+$; HR-ESIMS: m/z 201.0557 $[M + H]^+$ calcd for $C_{12}H_8O_3 + H^+$ (201.0552).

*4.3.2. 8-Acetyl-7-(prop-2-yn-1-yloxy)-2H-chromen-2-one (**9**).* White powder; yield, 79%; m.p. 155−157 °C; IR ($CHCl_3$) ν_{max} (cm^{-1}): 1722 (C═O), 1122 (C−O), 1324 (C−N); ^{1}H NMR (400 MHz, $CDCl_3$): δ (ppm) 7.67 (d, J = 8.7 Hz, 1H), 7.50 (d, J = 8.7 Hz, 1H), 7.05 (d, J = 8.6 Hz, 2H), 6.31 (d, J = 8.8 Hz, 1H), 4.82 (s, 2H), 2.62 (s, 3H), 2.58 (t, J = 2.4 Hz, 1H); ^{13}C NMR (100 MHz, $CDCl_3$): δ (ppm) 198.92, 159.57, 156.19, 151.43, 143.37, 129.62, 120.47, 114.42, 113.41, 109.38, 56.56, 32.37; ESIMS: m/z 243.06 $[M + H]^+$; HR-ESIMS: m/z 243.0657 $[M + H]^+$ calcd for $C_{14}H_{11}O_4 + H^+$ (243.0669).

*4.3.3. 4-Methyl-6,7-bis(prop-2-yn-1-yloxy)-2H-chromen-2-one (**12**).* Light brown powder; yield, 77%; m.p. 183−184 °C; IR ($CHCl_3$) ν_{max} (cm^{-1}): 1714 (C═O), 1183 (C−O), ^{1}H NMR (400 MHz, $CDCl_3$): δ (ppm) 7.23 (s, 1H), 7.05 (s, 1H), 6.20 (s, 1H), 4.84 (d, J = 2.4 Hz, 2H), 4.82 (d, J = 2.3 Hz, 2H), 2.59 (t, J = 2.5 Hz, 1H), 2.57 (t, J = 2.4 Hz, 1H), 2.41 (s, 3H); ^{13}C NMR (100 MHz, $CDCl_3$): δ (ppm) 161.02, 152.53, 151.57, 149.80, 144.13, 113.58, 113.05, 110.11, 102.66, 78.08, 57.46, 56.50, 18.50; ESIMS: m/z 269.08 $[M + H]^+$; HR-ESIMS: m/z 269.0830 $[M + H]^+$ calcd for $C_{16}H_{12}O_4 + H^+$ (269.0814).

*4.3.4. 6-Methoxy-4-methyl-7-(prop-2-yn-1-yloxy)-2H-chromen-2-one (**15**).* Light brown powder; m.p. 177−179 °C; IR ($CHCl_3$) ν_{max} (cm^{-1}): 1723 (C═O), 1159 (C−O); ^{1}H NMR (400 MHz, $CDCl_3$): δ (ppm) 7.03 (s, 1H), 6.97 (s, 1H), 6.20 (s, 1H), 4.84 (d, J = 2.4 Hz, 2H), 3.94 (s, 3H), 2.60 (t, J = 2.4 Hz, 1H), 2.42 (d, J = 3.4 Hz, 3H); ^{13}C NMR (100 MHz, $CDCl_3$): δ (ppm) 161.87, 152.51, 150.43, 149.11, 146.76, 113.79, 113.10, 106.03, 102.66, 56.92, 55.93, 18.52; ESIMS: m/z 245.2 $[M + H]^+$; HR-ESIMS: m/z 245.0825 $[M + H]^+$ calcd for $C_{14}H_{12}O_4 + H^+$ (245.0814).

*4.3.5. 7-(Prop-2-yn-1-yloxy)-2H-chromen-2-one (**18**).* Yellowish brown powder; yield, 91%; m.p. 114−115 °C; IR ($CHCl_3$) ν_{max} (cm^{-1}): 1726 (C═O), 1673, 1160 (C−O), ^{1}H NMR (400 MHz, $CDCl_3$): δ (ppm) 7.67 (d, J = 14.7 Hz, 1H), 7.42 (d, J = 13.7 Hz, 1H), 6.94−6.90 (m, 2H), 6.29 (d, J = 12.4 Hz, 1H), 4.77 (d, J = 2.0 Hz, 2H), 2.59 (t, J = 2.4 Hz, 1H); ^{13}C NMR (100 MHz, $CDCl_3$): δ (ppm) 161.18, 160.18, 155.81, 143.29, 128.85, 113.67, 113.20, 113.06, 102.35, 56.22; ESIMS: m/z 201.05 $[M + H]^+$; HR-ESIMS: m/z 201.0561 $[M + H]^+$ calcd for $C_{12}H_8O_3 + H^+$ (201.0552).

4.4. General Procedure for the Synthesis of Triazoles 8a−o, 10a−d, 13a−d, 16a−d, and 19a−d. To a round-bottom flask, substituted benzyl bromide (7) (1.5 equiv), triethylamine (0.3 equiv), and sodium azide (1.5 equiv) were *taken in tert*-butanol/water (1:1). This mixture was stirred at room temperature for half an hour. After half an hour, propargylated coumarin **6**, **9**, **12**, **15**, or **18** (1.5 equiv) was added along with sodium ascorbate (0.2 equiv) and copper sulfate (0.1 equiv), and the reaction was stirred for 24 h. Then, 30 mL water was added and extraction was done with EtOAc (3 × 50 mL). The three layers are combined and concentrated on a vacuum rotary evaporator. Thus, the residue was purified by column chromatography (solvent system: 40% EtOAc in hexane for **8a−o** and **19a−d** and 70% EtOAc in hexane for **10a−d**, **13a−d**, and **16a−d**) to obtain final triazoles.

*4.4.1. 4-((1-Benzyl-1H-1,2,3-triazol-4-yl)methoxy)-2H-chromen-2-one (**8a**).* Off-white coarse powder; yield, 82%; m.p. 176−177 °C; IR (KBr) ν_{max} (cm^{-1}): 1715 (C═O), 1238 (C−O), 1376 (C−N); ^{1}H NMR (400 MHz, $CDCl_3$) δ (ppm): 7.78 (s, 2H), 7.76 (d, J = 13 Hz, 1H), 7.56−7.53 (m, 1H), 7.43−7.37 (m, 1H), 7.31 (dd, J = 8.4, 1.4 Hz, 1H), 7.24−7.22 (m, 1H), 7.03−6.99 (m, 3H), 5.85 (s, 1H), 5.69 (s, 2H), 5.30 (s, 2H); ^{13}C NMR (100 MHz, $CDCl_3$): δ (ppm) 165.03, 162.46, 159.39, 153.23, 141.61, 132.57, 131.73, 124.31, 123.79, 122.75, 117.85, 116.28, 112.94, 91.24, 62.39, 41.98. ESIMS: m/z 334.11 $[M + H]^+$; HR-ESIMS: m/z 334.1197 $[M + H]^+$ calcd for $C_{19}H_{15}N_3O_3 + H^+$ (334.1192).

*4.4.2. 4-((1-(2-Chlorobenzyl)-1H-1,2,3-triazol-4-yl)-methoxy)-2H-chromen-2-one (**8b**).* White powder; yield, 67%; m.p. 162−163 °C; IR ($CHCl_3$) ν_{max} (cm^{-1}): 1715 (C═O), 767 (C−Cl), 1187 (C−O), 1273 (C−N); ^{1}H NMR (400 MHz, $CDCl_3$): δ (ppm) 7.79 (s, 1H, triazole), 7.77 (d, J

https://doi.org/10.1021/acsomega.2c07993
ACS Omega 2023, 8, 11161−11176

= 8.1 Hz, 1H), 7.55−7.51 (m, 1H), 7.45−7.44 (m, 1H), 7.37−7.33 (m, 1H), 7.31−7.29 (m, 3H), 7.25 (t, J = 4.3 Hz, 1H), 5.85 (s, 1H), 5.72 (s, 2H), 5.32 (s, 2H); ^{13}C NMR (100 MHz, $CDCl_3$): δ (ppm) 164.86, 162.65, 153.31, 142.01, 133.54, 132.40, 130.43, 129.86, 129.28, 127.32, 123.93, 123.65, 123.09, 117.13, 115.17, 91.16, 62.86, 51.87; ESIMS: m/z 368.08 $[M + H]^+$; HR-ESIMS: m/z 368.0810 $[M + H]^+$ calcd for $C_{19}H_{14}ClN_3O_3 + H^+$ (368.0802).

*4.4.3. 4-((1-(3-Chlorobenzyl)-1H-1,2,3-triazol-4-yl)-methoxy)-2H-chromen-2-one (**8c**).* White powder; yield, 71%; m.p. 198−199 °C; IR ($CHCl_3$) ν_{max} (cm^{-1}): 1716 (C═O), 761 (C−Cl), 1214 (C−O), 1377 (C−N); ^{1}H NMR (400 MHz, $CDCl_3$): δ (ppm) 7.78 (dd, J = 8.0, 4.0 Hz, 1H), 7.69 (s, 1H, triazole), 7.56−7.52 (m, 1H), 7.37−7.34 (m, 2H), 7.32−7.29 (m, 2H), 7.25 (d, J = 6.8 Hz, 1H), 7.21 (d, J = 6.5 Hz, 1H), 5.85 (s, 1H), 5.57 (s, 2H), 5.33 (s, 2H); ^{13}C NMR (100 MHz, $CDCl_3$): δ (ppm) 164.85, 162.45, 153.25, 142.17, 132.60, 130.59, 129.26, 128.25, 126.24, 123.95, 123.42, 123.17, 116.91, 115.46, 91.46, 62.60, 53.51; ESIMS: m/z 368.08 $[M + H]^+$; HR-ESIMS: m/z 368.0809 $[M + H]^+$ calcd for $C_{19}H_{14}ClN_3O_3 + H^+$ (368.0802).

*4.4.4. 4-((1-(2,6-Dichlorobenzyl)-1H-1,2,3-triazol-4-yl)-methoxy)-2H-chromen-2-one (**8d**).* Yellowish orange powder; yield, 74%; m.p. 174−175 °C; IR ($CHCl_3$) ν_{max} (cm^{-1}): 1716 (C═O), 761 (C−Cl), 1215 (C−O), 1377 (C−N); ^{1}H NMR (400 MHz, $CDCl_3$): δ (ppm) 7.77 (dd, J = 8.0, 4.0 Hz, 1H), 7.72 (s, 1H, triazole), 7.54−7.52 (m, 1H), 7.45 (d, J = 7.9 Hz, 1H), 7.43 (s, 1H), 7.35−7.30 (m, 2H), 7.25−7.21 (m, 1H), 5.92 (s, 1H), 5.85 (s, 2H), 5.29 (s, 2H); ^{13}C NMR (100 MHz, $CDCl_3$): δ (ppm) 164.92, 162.40, 153.83, 141.31, 136.83, 132.29, 131.05, 129.79, 129.53, 124.30, 123.46, 123.23, 122.99, 117.00, 115.47, 91.21, 62.81, 49.25; ESIMS: m/z 402.04 $[M + H]^+$; HR-ESIMS: m/z 402.0415 $[M + H]^+$ calcd for $C_{19}H_{13}Cl_2N_3O_3 + H^+$ (402.0412).

*4.4.5. 4-((1-(2-Fluorobenzyl)-1H-1,2,3-triazol-4-yl)-methoxy)-2H-chromen-2-one (**8e**).* Pale white powder; yield, 65%; m.p. 182−183 °C; IR ($CHCl_3$) ν_{max} (cm^{-1}): 1713 (C═O), 1452 (C−F), 1215 (C−O), 1377 (C−N); ^{1}H NMR (400 MHz, $CDCl_3$): δ (ppm) 7.77 (d, J = 8 Hz, 1H), 7.63 (s, 1H, triazole), 7.56 (t, J = 4 Hz, 1H), 7.34−7.32 (m, 3H), 7.24 (d, J = 8 Hz, 1H), 7.12 (t, J = 7.4 Hz, 2H), 5.84 (s, 1H), 5.56 (s, 2H), 5.32 (s, 2H); ^{13}C NMR (100 MHz, $CDCl_3$): δ (ppm) 164.97, 164.25 (d, $^1J_{C-F}$ = 279 Hz), 162.66, 153.35, 141.96, 132.61, 130.20 (d, $^3J_{C-F}$ = 9 Hz), 129.99, 123.94, 123.16, 116.82, 116.46 (d, $^2J_{C-F}$ = 21 Hz), 116.24, 115.41, 91.20, 62.61, 53.71; ESIMS: m/z 352.11 $[M + H]^+$; HR-ESIMS: m/z 352.1107 $[M + H]^+$ calcd for $C_{19}H_{14}FN_3O_3 + H^+$ (352.1097).

*4.4.6. 4-((1-(3-Fluorobenzyl)-1H-1,2,3-triazol-4-yl)-methoxy)-2H-chromen-2-one (**8f**).* White powder; yield, 83%; m.p. 173−175 °C; IR ($CHCl_3$) ν_{max} (cm^{-1}): 1714 (C═O), 1761 (C−F), 1266 (C−O), 1377 (C−N); ^{1}H NMR (400 MHz, $CDCl_3$): δ (ppm) 7.77 (dd, J = 8.0, 4.4 Hz, 1H), 7.63 (s, 1H, triazole), 7.57−7.53 (m, 3H), 7.34−7.30 (m, 1H), 7.12−7.09 (m, 2H), 5.84 (s, 1H), 5.56 (s, 2H), 5.32 (s, 2H); ^{13}C NMR (100 MHz, $CDCl_3$): δ (ppm) 164.97, 164.24 (d, $^1J_{C-F}$ = 247 Hz), 162.66, 152.33, 141.96, 132.61, 130.20 (d, $^3J_{C-F}$ = 8 Hz), 130.03 (d, $^4J_{C-F}$ = 3 Hz), 123.94, 123.20, 123.15, 116.81, 116.45 (d, $^2J_{C-F}$ = 21 Hz), 115.41, 91.19, 62.61, 53.71; ESIMS: m/z 352.11 $[M + H]^+$; HR-ESIMS: m/z 352.1103 $[M + H]^+$ calcd for $C_{19}H_{14}FN_3O_3 + H^+$ (352.1097).

*4.4.7. 4-((1-(4-Fluorobenzyl)-1H-1,2,3-triazol-4-yl)-methoxy)-2H-chromen-2-one (**8g**).* White powder; yield, 80%; m.p. 179−180 °C; IR ($CHCl_3$) ν_{max} (cm^{-1}): 1714 (C═O), 761 (C−F), 1188 (C−O), 1377 (C−N); ^{1}H NMR (400 MHz, $CDCl_3$): δ (ppm) 7.77 (d, J = 4.7 Hz, 1H), 7.62 (s, 1H, triazole), 7.57−7.53 (m, 1H), 7.34−7.29 (m, 3H), 7.23−7.21 (m, 1H), 7.12−7.10 (m, 2H), 5.84 (s, 1H), 5.56 (s, 2H), 5.32 (s, 2H); ^{13}C NMR (100 MHz, $CDCl_3$): δ (ppm) 164.99, 164.23 (d, $^1J_{C-F}$ = 247 Hz), 162.70, 153.24, 141.93, 132.61, 130.20 (d, $^3J_{C-F}$ = 8 Hz), 130.05 (d, $^4J_{C-F}$ = 4 Hz), 123.96, 123.27, 123.16, 116.78, 116.43 (d, $^2J_{C-F}$ = 8 Hz), 91.64, 62.60, 53.60; ESIMS: m/z 352.11 $[M + H]^+$; HR-ESIMS: m/z 352.1103 $[M + H]^+$ calcd for $C_{19}H_{14}FN_3O_3 + H^+$ (352.1097).

*4.4.8. 4-((1-(2,6-Difluorobenzyl)-1H-1,2,3-triazol-4-yl)-methoxy)-2H-chromen-2-one (**8h**).* White powder; yield, 70%; m.p. 176−178 °C; IR ($CHCl_3$) ν_{max} (cm^{-1}): 1715 (C═O), 1452 (C−F), 1272 (C−O), 1376 (C−N); ^{1}H NMR (400 MHz, $CDCl_3$): δ (ppm) 7.77 (dd, J = 8.0, 1.5 Hz, 1H), 7.64 (s, 1H), 7.56−7.52 (m, 1H), 7.41−7.38 (m, 2H), 7.33−7.30 (m, 2H), 7.24 (t, J = 7.6 Hz, 1H), 5.85 (s, 1H), 5.59 (s, 2H), 5.31 (s, 2H); ^{13}C NMR (100 MHz, $CDCl_3$): δ (ppm) 165.04, 162.76, 160.58 (d, $^1J_{C-F}$ = 243 Hz), 153.32, 141.81, 134.12, 132.60, 129.70, 129.07, 128.48,123.35, 123.16, 116.72, 115.42, 91.43, 62.64, 54.78; ESIMS: m/z 370.10 $[M + H]^+$; HR-ESIMS: m/z 370.1010 $[M + H]^+$ calcd for $C_{19}H_{13}F_2N_3O_3 + H^+$ (370.1003).

*4.4.9. 4-((1-(2-(Trifluoromethyl)benzyl)-1H-1,2,3-triazol-4-yl)methoxy)-2H-chromen-2-one (**8i**).* Cream powder; yield, 78%; m.p. 185−186 °C; IR ($CHCl_3$) ν_{max} (cm^{-1}): 1725 (C═O), 1454 (C−F), 1175 (C−O), 1334 (C−N); ^{1}H NMR (400 MHz, $CDCl_3$): δ (ppm) 7.76 (s, 1H, triazole), 7.74 (s, 2H), 7.60−7.56 (m, 1H), 7.54−7.48 (m, 2H), 7.31−7.28 (m, 2H), 7.25−7.19 (m, 1H), 5.86 (s, 1H), 5.80 (s, 2H), 5.33 (s, 2H); ^{13}C NMR (100 MHz, $CDCl_3$): δ (ppm) 164.96, 162.60, 153.34, 149.20, 138.10, 132.63, 131.48 (d, $^3J_{C-F}$ = 32 Hz), 128.38, 126.34 (q, $^4J_{C-F}$ = 7, 4 Hz), 125.06 (d, $^1J_{C-F}$ = 270 Hz), 123.95 (d, $^2J_{C-F}$ = 83 Hz), 123.44, 116.82, 115.39, 91.20, 62.59, 53.56; ESIMS: m/z 402.1 $[M + H]^+$; HR-ESIMS: m/z 402.1073 $[M + H]^+$ calcd for $C_{20}H_{14}F_3N_3O_3 + H^+$ (402.1066).

*4.4.10. 4-((1-(4-(Trifluoromethyl)benzyl)-1H-1,2,3-triazol-4-yl)methoxy)-2H-chromen-2-one (**8j**).* White powder; yield, 69%; m.p. 188−189 °C; IR ($CHCl_3$) ν_{max} (cm^{-1}): 1714 (C═O), 761 (C−F), 1280 (C−O), 1377 (C−N); ^{1}H NMR (400 MHz, $CDCl_3$): δ (ppm) 7.77 (d, J = 8.4 Hz, 1H), 7.63 (s, 1H, triazole), 7.57−7.53 (m, 1H), 7.34−7.30 (m, 3H), 7.24−7.21 (m, 1H), 7.13−7.07 (m, 2H), 5.84 (s, 1H), 5.56 (s, 2H), 5.32 (s, 2H); ^{13}C NMR (100 MHz, $CDCl_3$): δ (ppm) 164.98, 162.67, 161.78, 153.34, 141.95, 132.62, 130.20 (d, $^4J_{C-F}$ = 8 Hz), 129.99, 123.94, 123.17, 123.15, 116.82 (d, $^2J_{C-F}$ = 36 Hz), 116.24, 115.41, 91.20, 62.61, 53.71; ESIMS: m/z 402.10 $[M + H]^+$; HR-ESIMS: m/z 402.1071 $[M + H]^+$ calcd for $C_{20}H_{14}F_3N_3O_3 + H^+$ (402.1066).

*4.4.11. 4-((1-(2-(Trifluoromethoxy)benzyl)-1H-1,2,3-triazol-4-yl)methoxy)-2H-chromen-2-one (**8k**).* Light yellow powder; yield, 75%; m.p. 154−155 °C; IR ($CHCl_3$) ν_{max} (cm^{-1}): 1726 (C═O), 1458 (C−F), 1248 (C−O), 1275 (C−N); ^{1}H NMR (400 MHz, $CDCl_3$): δ (ppm) 7.77 (d, J = 9.2 Hz, 1H), 7.72 (s, 1H, triazole), 7.57−7.52 (m, 1H), 7.47−7.43 (m, 1H), 7.35−7.30 (t, J = 7.4 Hz, 4H), 7.25 (t, J = 6.9 Hz, 1H), 5.85 (s, 1H), 5.68 (s, 2H), 5.32 (s, 2H); ^{13}C NMR (100 MHz, $CDCl_3$): δ (ppm) 164.96, 162.63, 153.33, 149.61, 142.07, 132.87, 132.63, 129.79, 130.79 (d, $^3J_{C-F}$ = 36 Hz), 129.72, 123.95 (d, $^2J_{C-F}$ = 81 Hz), 123.36, 121.70, 121.63 (d,

https://doi.org/10.1021/acsomega.2c07993
ACS Omega 2023, 8, 11161−11176

$^{1}J_{C-F}$ = 256 Hz), 116.81, 115.39, 91.20, 62.59, 53.56; ESIMS: m/z 418.10 $[M + H]^+$; HR-ESIMS: m/z 418.1021 $[M + H]^+$ calcd for $C_{20}H_{14}F_3N_3O_4 + H^+$ (418.1015).

*4.4.12. 4-((1-(4-(Trifluoromethoxy)benzyl)-1H-1,2,3-triazol-4-yl)methoxy)-2H-chromen-2-one (**8l**).* White powder; yield, 78%; m.p. 165−167 °C; IR ($CHCl_3$) ν_{max} (cm^{-1}): 1727 (C═O), 1452 (C−F), 1243 (C−O), 1278 (C−N); ^1H NMR (400 MHz, dimethyl sulfoxide (DMSO)): δ (ppm) δ 8.49 (s, 1H, triazole), 7.74 (dd, J = 9.5, 4.5 Hz, 1H), 7.66−7.62 (m, 1H), 7.50−7.47 (m, 2H), 7.40−7.38 (m, 3H), 7.34−7.30 (m, 1H), 6.16 (s, 1H), 5.71 (s, 2H), 5.43 (s, 2H); ^{13}C NMR (100 MHz, DMSO): δ (ppm) 164.81, 162.04, 153.21, 148.59, 148.57, 141.83, 135.80, 133.27, 130.54, 125.98, 124.66, 123.32, 121.86, 121.75 (d, $^{1}J_{C-F}$ = 255 Hz), 116.91, 115.50, 91.78, 63.20, 52.50; ESIMS: m/z 418.1 $[M + H]^+$; HR-ESIMS: m/z 418.1015 $[M + H]^+$ calcd for $C_{20}H_{15}F_3N_3O_4F_3 + H^+$ (418.1015).

*4.4.13. 4-((1-(2-Methylbenzyl)-1H-1,2,3-triazol-4-yl)methoxy)-2H-chromen-2-one (**8m**).* Yellow powder; yield, 76%; m.p. 155−156 °C; IR ($CHCl_3$) ν_{max} (cm^{-1}): 1715 (C═O), 1261 (C−O), 1377 (C−N); ^1H NMR (400 MHz, $CDCl_3$): δ (ppm) 7.74 (d, J = 6.7 Hz, 1H), 7.59 (s, 1H, triazole), 7.54−7.50 (m, 1H), 7.32−7.29 (m, 2H), 7.25−7.20 (m, 4H), 5.83 (s, 1H), 5.60 (s, 2H), 5.28 (s, 2H), 2.31 (s, 3H); ^{13}C NMR (100 MHz, $CDCl_3$): δ (ppm) 165.03, 162.72, 153.25, 141.55, 136.98, 132.56, 132.13, 131.17, 129.55, 129.39, 126.80, 123.94, 123.43, 123.19, 116.70, 115.40, 91.09, 62.64, 52.58, 19.05, 18.83; ESIMS: m/z 348.1 $[M + H]^+$; HR-ESIMS: m/z 348.1345 $[M + H]^+$ calcd for $C_{20}H_{17}N_3O_3 + H^+$ (348.1348).

*4.4.14. 4-((1-(3-Methoxybenzyl)-1H-1,2,3-triazol-4-yl)methoxy)-2H-chromen-2-one (**8n**).* White powder; yield, 60%; m.p. 127−129 °C; IR ($CHCl_3$) ν_{max} (cm^{-1}): 1717 (C═O), 1159 (C−O), 1375 (C−N); ^1H NMR (400 MHz, $CDCl_3$): δ (ppm) 7.78 (dd, J = 7.4, 4.5 Hz, 1H), 7.64 (s, 1H), 7.56−7.52 (m, 1H), 7.34−7.30 (m, 2H), 7.27−7.21 (m, 1H), 6.92−6.88 (m, 2H), 6.84−6.83 (m, 1H), 5.84 (s, 1H), 5.55 (s, 2H), 5.31 (s, 2H), 3.80 (s, 3H); ^{13}C NMR (100 MHz, $CDCl_3$): δ (ppm) 164.95, 162.58, 159.88, 153.50, 142.37, 135.69, 132.57, 130.93, 124.23, 122.85, 120.17, 116.48, 115.08, 114.47, 114.09, 90.58, 62.66, 55.25, 54.24; ESIMS: m/z 364.1 $[M + H]^+$; HR-ESIMS: m/z 364.1297 $[M + H]^+$ calcd for $C_{20}H_{18}FN_3O_4 + H^+$ (364.1303).

*4.4.15. 4-((1-(3,5-Dimethoxybenzyl)-1H-1,2,3-triazol-4-yl)methoxy)-2H-chromen-2-one (**8o**).* Off-white powder; yield, 72%; m.p. 159−160 °C; IR ($CHCl_3$) ν_{max} (cm^{-1}): 1713 (C═O), 1226 (C−O), 1369 (C−N); ^1H NMR (400 MHz, $CDCl_3$): δ (ppm) 7.78 (d, J = 8.0 Hz, 1H), 7.65 (s, 1H, triazole), 7.57−7.53 (m, 1H), 7.32 (d, J = 5.0 Hz, 1H), 7.24 (d, J = 4.8 Hz, 1H), 6.45−6.43 (m, 3H), 5.84 (s, 1H), 5.50 (s, 2H), 5.33 (s, 2H), 3.78 (s, 6H); ^{13}C NMR (100 MHz, $CDCl_3$): δ (ppm) 165.01, 162.68, 161.41, 153.33, 141.83, 136.22, 132.58, 123.94, 123.38, 123.20, 116.79, 115.43, 106.25, 100.50, 91.16, 62.67, 55.48, 54.50; ESIMS: m/z 394.14 $[M + H]^+$; HR-ESIMS: m/z 394.1414 $[M + H]^+$ calcd for $C_{21}H_{19}N_3O_5 + H^+$ (394.1403).

*4.4.16. 4-((1-(4-Nitrobenzyl)-1H-1,2,3-triazol-4-yl)methoxy)-2H-chromen-2-one (**8p**).* Light yellow powder; yield, 75%; m.p. 193−194 °C; IR ($CHCl_3$) ν_{max} (cm^{-1}): 1731 (C═O), 1673, 1452 (NO_2), 1187 (C−O), 1377 (C−N); ^1H NMR (400 MHz, $CDCl_3$): δ (ppm) 8.28 (d, J = 1.8 Hz, 2H), 7.75 (dd, J = 7.4, 4.5 Hz, 1H), 7.71 (s, 1H), 7.60−7.54 (m, 1H), 7.46 (d, J = 1.9, 2H), 7.34−7.33 (m, 1H), 7.21−7.19 (m, 1H), 5.86 (s, 1H), 5.73 (s, 2H), 5.34 (s, 2H); ^{13}C NMR (100 MHz, $CDCl_3$): δ (ppm) 164.57, 162.52, 154.64, 153.26, 142.51, 141.21, 133.07, 124.90, 123.90, 123.62, 123.36, 116.78, 115.71, 90.76, 62.70, 52.69; ESIMS: m/z 379.10 $[M + H]^+$; HR-ESIMS: m/z 379.1046 $[M + H]^+$ calcd for $C_{19}H_{14}N_4O_5 + H^+$ (379.1042).

*4.4.17. 8-Acetyl-7-((1-(3-methoxybenzyl)-1H-1,2,3-triazol-4-yl)methoxy)-2H-chromen-2-one (**10a**).* Light orange powder; yield, 55%; m.p. 213−214 °C; IR ($CHCl_3$) ν_{max} (cm^{-1}): 1731 (C═O), 1141 (C−O), 1391 (C−N); ^1H NMR (400 MHz, $CDCl_3$): δ (ppm) 7.64 (d, J = 7.7 Hz, 1H), 7.57 (s, 1H, triazole), 7.47 (d, J = 7.7 Hz, 1H), 7.30 (d, J = 7.7 Hz, 1H), 7.11 (d, J = 4.0 Hz, 2H), 6.90−6.83 (m, 2H), 6.77 (s, 1H), 6.31 (d, J = 4.3 Hz, 1H), 5.49 (s, 2H), 5.31 (s, 2H), 3.78 (s, 3H), 2.55 (s, 3H); ^{13}C NMR (100 MHz, $CDCl_3$): δ (ppm) 198.91, 160.19, 159.88, 151.13, 143.03, 142.36, 135.31, 130.22, 129.60, 122.54, 119.86, 114.10, 113.10, 112.79, 109.41, 63.32, 55.28, 54.29, 32.04.; ESIMS: m/z 406.14 $[M + H]^+$; HR-ESIMS: m/z 406.1406 $[M + H]^+$ calcd for $C_{23}H_{20}N_3O_5 + H^+$ (406.1403).

*4.4.18. 8-Acetyl-7-((1-(3,5-dimethoxybenzyl)-1H-1,2,3-triazol-4-yl)methoxy)-2H-chromen-2-one (**10b**).* White powder; yield, 54%; m.p. 232−234 °C; IR ($CHCl_3$) ν_{max} (cm^{-1}): 1727 (C═O), 1142 (C−O), 1367 (C−N); ^1H NMR (400 MHz, $CDCl_3$): δ (ppm) 7.64 (d, J = 8.5 Hz, 1H), 7.58 (s, 1H, triazole), 7.45 (d, J = 8.7 Hz, 1H), 7.11 (d, J = 8.6 Hz, 1H), 6.43−6.41 (m, 1H), 6.38 (s, 2H), 6.30−6.27 (m, 1H), 5.42 (s, 2H), 5.29 (s, 2H), 3.76 (s, 6H), 2.56 (s, 3H); ^{13}C NMR (100 MHz, $CDCl_3$): δ (ppm) 199.32, 161.36, 159.73, 156.99, 151.56, 143.34, 142.82, 136.53, 129.71, 122.87, 120.15, 114.47, 113.34, 109.55, 106.24, 100.22, 62.87, 55.50, 54.66, 32.32.; ESIMS: m/z 436.15 $[M + H]^+$; HR-ESIMS: m/z 436.1509 $[M + H]^+$ calcd for $C_{23}H_{22}N_3O_6 + H^+$ (436.1508).

*4.4.19. 8-Acetyl-7-((1-(2-(trifluoromethyl)benzyl)-1H-1,2,3-triazol-4-yl)methoxy)-2H-chromen-2-one (**10c**).* Orange sticky powder; yield, 51%; IR ($CHCl_3$) ν_{max} (cm^{-1}): 1726 (C═O), 1185 (C−O), 1315 (C−N), 1255 (C−F); ^1H NMR (400 MHz, $CDCl_3$): δ (ppm) 7.65 (d, J = 12 Hz, 2H), 7.46−7.41 (m, 2H), 7.33−7.30 (m, 2H), 7.28−7.27 (m, 1H), 7.11 (d, J = 12 Hz, 1H), 6.30 (d, J = 8 Hz, 1H), 5.62 (s, 2H), 5.32 (s, 2H), 2.56 (s, 3H); ^{13}C NMR (100 MHz, $CDCl_3$): δ (ppm) 198.93, 159.71, 157.17, 151.26, 143.38, 143.00, 130.91, 130.67, 130.49, 129.69, 128.82 (d, $^{1}J_{C-F}$ = 242 Hz), 127.49, 123.38, 120.63, 114.27, 113.37, 109.56, 63.16, 48.69, 32.43; ESIMS: m/z 444.1 $[M + H]^+$; HR-ESIMS: m/z 444.1160 $[M + H]^+$ calcd for $C_{22}H_{17}N_3O_4F_3 + H^+$ (444.1171).

*4.4.20. 8-Acetyl-7-((1-(2-(trifluoromethoxy)benzyl)-1H-1,2,3-triazol-4-yl)methoxy)-2H-chromen-2-one (**10d**).* Reddish sticky powder; yield, 52%; IR ($CHCl_3$) ν_{max} (cm^{-1}): 1728 (C═O), 1187 (C−O), 1312 (C−N), 1124 (C−F); ^1H NMR (400 MHz, $CDCl_3$): δ (ppm) 7.64−7.62 (m, 2H), 7.46−7.40 (m, 2H), 7.32−7.30 (m, 2H), 7.26−7.24 (m, 1H), 7.11 (d, J = 7.7 Hz, 1H), 6.30 (d, J = 9.6 Hz, 1H), 5.62 (s, 2H), 5.32 (s, 2H), 2.56 (s, 3H). ^{13}C NMR (100 MHz, $CDCl_3$): δ (ppm) 198.95, 159.73, 157.16, 151.25, 143.37, 143.01, 130.67 (d, $^{3}J_{C-F}$ = 18 Hz), 129.69 (d, $^{1}J_{C-F}$ = 219 Hz), 126.39, 120.62, 120.01, 114.26, 113.37, 109.55, 63.15, 48.69, 32.44; ESIMS: m/z 460.1 $[M + H]^+$; HR-ESIMS: m/z 460.1118 $[M + H]^+$ calcd for $C_{22}H_{17}N_3O_5F_3 + H^+$ (460.1120).

*4.4.21. 6,7-Bis((1-(3-methoxybenzyl)-1H-1,2,3-triazol-4-yl)methoxy)-4-methyl-2H-chromen-2-one (**13a**).* Yellowish oil; yield, 64%; m.p. 129−131 °C; IR ($CHCl_3$) ν_{max} (cm^{-1}): 1712 (C═O), (NO_2), 1162 (C−O), 1388 (C−N); ^1H NMR

https://doi.org/10.1021/acsomega.2c07993
ACS Omega 2023, 8, 11161−11176

(400 MHz, $CDCl_3$): δ (ppm) δ 7.55 (d, J = 9.8 Hz, 2H), 7.23−7.21 (m, 1H), 7.19 (s, 1H), 7.17 (s, 1H), 6.87 (s, 2H), 6.83−6.78 (m, 3H), 6.75−6.72 (m, 2H), 6.69−6.68 (m, 1H), 6.08 (s, 1H), 5.41 (d, J = 9.1 Hz, 4H), 5.18 (d, J = 13.2 Hz, 4H), 3.70 (s, 6H), 2.28 (s 3H); ^{13}C NMR (100 MHz, $CDCl_3$): δ (ppm) 161.27, 160.12, 152.45, 152.08, 149.72, 144.67, 144.01, 135.92, 135.78, 130.28, 130.22, 123.42, 123.27, 120.35, 120.24, 114.29, 114.09, 113.83, 113.80, 113.35, 112.66, 111.01, 102.24, 64.21, 63.00, 55.33, 54.23, 18.86; ESIMS: m/z 595.2 $[M + H]^+$; HR-ESIMS: m/z 595.2297 $[M + H]^+$ calcd for $C_{32}H_{31}N_6O_6 + H^+$ (595.2305).

*4.4.22. 6,7-Bis((1-(3,5-dimethoxybenzyl)-1H-1,2,3-triazol-4-yl)methoxy)-4-methyl-2H-chromen-2-one (**13b**).* Light yellow powder; yield, 61%; m.p. 124−126 °C; IR ($CHCl_3$) ν_{max} (cm^{-1}): 1711 (C═O), 1159 (C−O), 1430 (C−N); ^{1}H NMR (400 MHz, $CDCl_3$): δ (ppm) 7.56 (d, J = 8.1 Hz, 2H), 7.17 (s,1H), 6.87 (s, 1H, triazole), 6.35−6.33 (m, 4H), 6.29 (d, J = 2.2 Hz, 2H), 6.08 (d, J = 1.1 Hz, 1H), 5.37 (d, J = 9.0 Hz, 4H), 5.19 (d, J = 11.5 Hz, 4H), 3.67 (s, 12H), 2.28 (d, J = 1.0 Hz, 3H); ^{13}C NMR (100 MHz, $CDCl_3$): δ (ppm) 161.34, 161.31, 161.26, 152.44, 152.08, 149.72, 144.66, 144.02, 143.09, 136.60, 136.46, 123.43, 123.27, 113.34, 112.64, 110.97, 106.17, 106.12, 102.22, 100.48, 100.28, 64.21, 63.00, 55.44, 54.24, 18.85; ESIMS: m/z 655.2 $[M + H]^+$; HR-ESIMS: m/z 655.2520 $[M + H]^+$ calcd for $C_{34}H_{35}N_6O_8 + H^+$ (655.2516).

*4.4.23. 4-Methyl-6,7-bis((1-(2-(trifluoromethyl)benzyl)-1H-1,2,3-triazol-4-yl)methoxy)-2H-chromen-2-one (**13c**).* Pale yellow powder; yield, 74%; m.p. 168−170 °C; IR ($CHCl_3$) ν_{max} (cm^{-1}): 1728 (C═O), 1673, 1452 (NO_2), 1163 (C−O), 1314 (C−N), 1062 (C−F); ^{1}H NMR (400 MHz, $CDCl_3$): δ (ppm) 7.73 (d, J = 8.1 Hz, 2H), 7.65 (d, J = 8.2 Hz, 2H), 7.54−7.49 (m,2H), 7.46−7.44 (m, 3H), 7.24 (s, 1H), 7.20 (d, J = 1.2 Hz, 1H), 7.16 (d, J = 7.7 Hz, 1H), 6.96 (s, 1H), 6.16 (d, J = 1.2 Hz, 1H), 5.73 (d, J = 7.8 Hz, 4H), 5.28 (d, J = 9.8 Hz, 4H), 2.36 (s, 3H); ^{13}C NMR (100 MHz, $CDCl_3$): δ (ppm) 161.19, 152.34, 152.05, 149.75, 144.69, 144.16, 143.29, 132.79, 132.69, 130.27, 130.19, 128.89, 128.16 (d, $^2J_{C-F}$ = 31 Hz), 126.32 (q, $^4J_{C-F}$ = 6 Hz), 125.45 (d, $^1J_{C-F}$ = 272 Hz), 123.79 (d, $^3J_{C-F}$ = 15 Hz), 113.41, 112.75, 110.99, 102.39, 64.08, 63.02, 50.26, 18.81. ESIMS: m/z 671.18 $[M + H]^+$; HR-ESIMS: m/z 671.1832 $[M + H]^+$ calcd for $C_{32}H_{25}N_6O_4F_6 + H^+$ (671.1841).

*4.4.24. 4-Methyl-6,7-bis((1-(2-(trifluoromethoxy)benzyl)-1H-1,2,3-triazol-4-yl)methoxy)-2H-chromen-2-one (**13d**).* Light brown powder; yield, 78%; m.p. 173−174 °C; IR ($CHCl_3$) ν_{max} (cm^{-1}): 1724 (C═O), 1184 (C−O), 1339 (C−N) 1070 (C−F); ^{1}H NMR (400 MHz, $CDCl_3$): δ (ppm) 7.67 (d, J = 8.0 Hz, 2H), 7.44−7.38 (m, 2H), 7.33−7.31 (m, 2H), 7.29 (s, 1H), 7.25 (s, 2H), 7.24−7.23 (m, 1H), 7.20−7.10 (m, 1H), 6.96 (s, 1H), 6.16 (d, J = 1.2 Hz, 1H), 5.63 (d, J = 7.8 Hz, 4H), 5.28 (d, J = 9.8 Hz, 4H), 2.35 (s, 3H); ^{13}C NMR (100 MHz, $CDCl_3$): δ (ppm) 161.25, 152.40, 152.01, 149.71, 146.94, 144.67, 144.06, 130.58, 130.55, 130.50 (d, $^3J_{C-F}$ = 11Hz), 130.39, 127.54 (d, $^4J_{C-F}$ = 8 Hz), 127.12 (d, $^4J_{C-F}$ = 8 Hz), 123.66 (d, $^2J_{C-F}$ = 16 Hz), 120.63, 113.38, 112.71, 110.88, 102.34, 64.01, 62.98, 48.49, 18.82; ESIMS: m/z 703.1 $[M + H]^+$; HR-ESIMS: m/z 703.1733 $[M + H]^+$ calcd for $C_{32}H_{25}N_6O_4F_6 + H^+$ (703.1740).

*4.4.25. 6-Methoxy-7-((1-(3-methoxybenzyl)-1H-1,2,3-triazol-4-yl)methoxy)-4-methyl-2H-chromen-2-one (**16a**).* Light yellow powder; yield, 70%; m.p. 159−161 °C; IR ($CHCl_3$) ν_{max} (cm^{-1}): 1713 (C═O), 1275 (C−O), 1381 (C−N); ^{1}H NMR (400 MHz, $CDCl_3$): δ (ppm) 7.61 (s, 1H, triazole), 7.31−7.27 (m, 1H), 7.00 (s, 1H), 6.93 (s, 1H), 6.91−6.85 (m, 2H), 6.80−6.78 (m, 1H), 6.17 (s, 1H), 5.50 (s, 2H), 5.28 (s, 2H), 3.89 (s, 3H), 3.78 (s, 3H), 2.40 (s, 3H); ^{13}C NMR (100 MHz, $CDCl_3$): δ (ppm) 161.38, 161.34, 152.19, 151.20, 149.07, 146.45, 143.17, 136.36, 123.13, 113.11, 112.68, 106.20, 105.59, 101.94, 100.55, 63.07, 56.47, 55.46, 54.39, 18.91; ESIMS: m/z 408.1 $[M + H]^+$; HR-ESIMS: m/z 408.1566 $[M + H]^+$ calcd for $C_{12}H_{21}N_3O_5 + H^+$ (408.1559).

*4.4.26. 7-((1-(3,5-Dimethoxybenzyl)-1H-1,2,3-triazol-4-yl)-methoxy)-6-methoxy-4-methyl-2H-chromen-2-one (**16b**).* White powder; yield, 71%; m.p. 151−152 °C; IR ($CHCl_3$) ν_{max} (cm^{-1}): 1728 (C═O), 1123 (C−O), 1350 (C−N); ^{1}H NMR (400 MHz, $CDCl_3$): δ (ppm) 7.61 (s, 1H, triazole), 7.03 (s, 1H), 6.93 (s, 1H), 6.43 (s, 1H), 6.37 (s, 2H), 6.18 (s, 1H), 5.45 (s, 2H), 5.29 (s, 2H), 3.89 (s, 3H), 3.76 (s, 6H), 2.40 (s, 3H); ^{13}C NMR (100 MHz, $CDCl_3$): δ (ppm) 161.23, 151.92, 151.16, 148.87, 146.62, 143.10, 136.03, 123.20, 113.07, 112.84, 106.56, 105.75, 101.49, 100.75, 63.17, 56.37, 55.63, 54.38, 19.08; ESIMS: m/z 438.1 $[M + H]^+$; HR-ESIMS: m/z 438.1659 $[M + H]^+$ calcd for $C_{23}H_{23}N_3O_6 + H^+$ (438.1665).

*4.4.27. 6-Methoxy-4-methyl-7-((1-(2-(trifluoromethyl)-benzyl)-1H-1,2,3-triazol-4-yl)methoxy)-2H-chromen-2-one (**16c**).* White powder; yield, 70%; m.p. 151−153 °C; IR ($CHCl_3$) ν_{max} (cm^{-1}): 1727 (C═O), 1273 (C−O), 1427 (C−N); ^{1}H NMR (400 MHz, $CDCl_3$): δ (ppm) 7.67 (d, J = 8.5 Hz, 1H), 7.57 (s, 1H, triazole), 7.49−7.46 (m, 1H), 7.42−7.38 (m, 1H), 7.17 (s, 1H), 6.95 (s, 1H), 6.87 (s, 1H), 6.12 (s, 1H), 5.68 (s, 2H), 5.24 (s, 2H), 3.83 (s, 3H), 2.34 (s, 3H); ^{13}C NMR (100 MHz, $CDCl_3$): δ (ppm) 161.37, 152.16, 151.16, 149.06, 146.48, 143.44, 132.82, 130.39, 128.91, 123.16 (d, $^1J_{C-F}$ = 274 Hz), 113.21, 112.76, 105.65, 102.11, 63.09, 56.49, 49.68, 18.91; ESIMS: m/z 446.1 $[M + H]^+$; HR-ESIMS: m/z 446.1330 $[M + H]^+$ calcd for $C_{22}H_{18}N_3O_4F_3 + H^+$ (446.1328).

*4.4.28. 6-Methoxy-4-methyl-7-((1-(2-(trifluoromethoxy)-benzyl)-1H-1,2,3-triazol-4-yl)methoxy)-2H-chromen-2-one (**16d**).* White powder; yield, 79%; m.p. 164−166 °C; IR ($CHCl_3$) ν_{max} (cm^{-1}): 1718 (C═O), 1275 (C−O), 1385 (C−N); ^{1}H NMR (400 MHz, $CDCl_3$): δ (ppm) 7.66 (s, 1H, triazole), 7.44−7.40 (m, 1H), 7.33−7.27 (m, 3H), 7.02 (s, 1H), 6.94 (s, 1H), 6.18 (s, 1H), 5.63 (s, 2H), 5.30 (s, 2H), 3.90 (s, 3H), 2.41 (s, 3H); ^{13}C NMR (100 MHz, $CDCl_3$): δ (ppm) 161.39, 152.21, 151.16, 149.05, 146.93, 146.46, 143.28, 130.60, 127.56, 127.03, 123.45 (d, $^1J_{C-F}$ = 257 Hz), 120.63, 113.16, 112.70, 105.61, 102.00, 63.03, 56.48, 48.47, 18.92. ESIMS: m/z 462.1 $[M + H]^+$; HR-ESIMS: m/z 462.1265 $[M + H]^+$ calcd for $C_{22}H_{19}N_3O_5F_3 + H^+$ (462.1277).

*4.4.29. 7-((1-(3-Methoxybenzyl)-1H-1,2,3-triazol-4-yl)-methoxy)-2H-chromen-2-one (**19a**).* White powder; yield, 70%; m.p. 137−138 °C; IR ($CHCl_3$) ν_{max} (cm^{-1}): 1725 (C═O), 1156 (C−O), 1305 (C−N); ^{1}H NMR (400 MHz, $CDCl_3$): δ (ppm) 7.64 (d, J = 9.5 Hz, 1H), 7.60 (s, 1H, triazole), 7.38 (d, J = 8.4 Hz, 1H), 7.31 (d, J = 7.5 Hz, 1H), 6.92−6.86 (m, 4H), 6.81 (t, J = 4.5 Hz, 1H), 6.26 (d, J = 9.5 Hz, 1H), 5.52 (s, 2H), 5.22 (s, 2H), 3.78 (s, 3H); ^{13}C NMR (100 MHz, $CDCl_3$): δ (ppm) 161.67, 160.95, 160.19, 155.93, 143.75, 135.76, 130.78, 129.01, 123.01, 120.08, 114.27, 113.83, 113.44, 112.98, 112.77, 101.59, 62.23, 55.51, 53.83. ESIMS: m/z 364.1 $[M + H]^+$; HR-ESIMS: m/z 364.1303 $[M + H]^+$ calcd for $C_{20}H_{17}N_3O_4 + H^+$ (364.1297).

*4.4.30. 7-((1-(3,5-Dimethoxybenzyl)-1H-1,2,3-triazol-4-yl)-methoxy)-2H-chromen-2-one (**19b**).* Light yellow powder; yield, 69%; m.p. 132−133 °C; IR ($CHCl_3$) ν_{max} (cm^{-1}): 1728 (C═O), 1120 (C−O), 1277 (C−N); ^{1}H NMR (400 MHz,

https://doi.org/10.1021/acsomega.2c07993
ACS Omega 2023, 8, 11161−11176

$CDCl_3$): δ (ppm) 7.65 (d, J = 9.5 Hz, 1H), 7.59 (s, 1H, triazole), 7.39 (d, J = 7.9 Hz, 1H), 6.93−6.90 (m, 2H), 6.44−6.43 (m, 1H), 6.41 (d, J = 7.8 Hz, 1H), 6.28 (d, J = 7.4 Hz, 1H), 5.47 (s, 2H), 5.23 (s, 2H), 3.76 (s, 6H); ^{13}C NMR (100 MHz, $CDCl_3$): δ (ppm) 161.37, 161.30, 161.09, 155.50, 143.38, 136.30, 128.91, 122.85, 113.49, 113.00, 112,78, 106.20, 102.08, 100.47, 61.94, 55.25, 54.25. ESIMS: m/z 394.14 $[M + H]^+$; HR-ESIMS: m/z 394.1406 $[M + H]^+$ calcd for $C_{21}H1_9N_3O_5 + H^+$ (394.1403).

*4.4.31. 7-((1-(2-(Trifluoromethyl)benzyl)-1H-1,2,3-triazol-4-yl)methoxy)-2H-chromen-2-one (**19c**).* Dark brown powder; yield, 67%; m.p. 119−121 °C; IR ($CHCl_3$) ν_{max} (cm^{-1}): 1731 (C═O), 1673, 1452 (NO_2), 1187 (C−O), 1377 (C−N); ^{1}H NMR (400 MHz, $CDCl_3$): δ (ppm) 7.74 (d, J = 7.8 Hz, 1H), 7.68 (s, 1H, triazole), 7.65 (d, J = 9.5 Hz, 1H), 7.56−7.53 (m, 1H), 7.49−7.46 (m, 1H), 7.40 (d, J = 8.5 Hz, 1H), 7.25 (d, J = 7.6 Hz, 1H), 6.93−6.91 (m, 1H), 6.89−6.88 (m, 1H), 6.26 (d, J = 9.5 Hz, 1H), 5.77 (s, 2H), 5.25 (s, 2H). ^{13}C NMR (100 MHz, $CDCl_3$): δ (ppm) 161.26, 161.05, 155.66, 143.51, 143.38, 132.79, 130.28, 128.95 (d, $^3J_{C-F}$ = 3 Hz), 128.13 (d, $^2J_{C-F}$ = 30 Hz), 126.37 (q, $^4J_{C-F}$ = 12, 6 Hz), 125.44 (d, $^1J_{C-F}$ = 272 Hz), 123.54, 113.41, 113.00, 112.77, 102.02, 62.25, 50.32. ESIMS: m/z 402.1 $[M + H]^+$; HR-ESIMS: m/z 402.1076 $[M + H]^+$ calcd for $C_{20}H_{14}N_3O_3F_3 + H^+$ (402.1066).

*4.4.32. 7-((1-(2-(Trifluoromethoxy)benzyl)-1H-1,2,3-triazol-4-yl)methoxy)-2H-chromen-2-one (**19d**).* Pale white powder; yield, 62%; m.p. 123−124 °C; IR ($CHCl_3$) ν_{max} (cm^{-1}): 1723 (C═O), 1124 (C−O), 1274 (C−N); ^{1}H NMR (400 MHz, $CDCl_3$): δ (ppm) 7.78 (d, J = 7.9 Hz, 1H), 7.74 (s, 1H, triazole), 7.57−7.53 (m, 1H), 7.48−7.43 (m, 1H), 7.37−7.34 (m, 3H), 7.33 (d, J = 7.5 Hz, 1H), 7.27−7.23 (m, 1H), 5.87 (s, 1H), 5.69 (s, 2H), 5.34 (s, 2H); ^{13}C NMR (100 MHz, $CDCl_3$): δ (ppm) 164.99, 162.64, 153.32, 147.04, 141.89, 132.57, 130.77 (d, $^4J_{C-F}$ = 8.08 Hz), 127.60, 126.82, 123.93, 123.70, 123.14, 121.76 (d, $^1J_{C-F}$ = 259.76 Hz), 120.65, 116.76, 115.41, 91.17, 62.61, 48.70; ESIMS: m/z 418.1 $[M + H]^+$; HR-ESIMS: m/z 418.1006 $[M + H]^+$ calcd for $C_{20}H_{14}N_3O_4F_3 + H^+$ (418.1015).

4.5. *In Vitro* AChE and BChE Inhibition Assay. The cholinesterase inhibition experiments, including the enzyme kinetics, were evaluated by Ellman assay as described earlier.[32]

4.6. *In Vitro* BACE-1 Inhibition Assay. The fluorescence resonance energy transfer (FRET) assay was used to screen all synthesized compounds[24] for BACE-1 inhibition and its enzyme kinetics.

4.7. Molecular Modeling. The Schrodinger software was used to carry out the molecular docking study. The crystal structures of human AChE (PDB ID: 4EY7),[33] human BChE (PDB ID: 6EP4),[34] and human BACE-1 (PDB ID: 1W51)[35] were obtained from the RCSB Protein Data Bank. The protocols employed were as given under the default settings of glide. Further, MD simulation was carried out using Desmond software (v 3.8) for 50 ns by a similar protocol as used in the previous publication of our group.[20]

4.8. Aβ-42 Self-Aggregation Inhibition Assay. The fluffy white solid obtained by pretreatment of amyloid β 1−42 peptide (PP69, Sigma) was reconstituted to produce a 200 mM solution in a mixture of ACN/Na_2CO_3/NaOH in a ratio of 48.4:48.4:3.2. The Aβ aliquots with and without test inhibitors were incubated for 24 h at 30 °C. thioflavin T (ThT) fluorescence method was used to assess the aggregates.[36]

4.9. *In Vitro* PAMPA−BBB Assay. The samples were diluted with PBS (pH 7.4). The acceptor plate wells were filled with 300 μL of PBS. The 4 μL of 20 mg/mL porcine brain lipid (PBL) in dodecane was used to coat the permeable layer of the donor plate. The test compounds were added to the donor plate. The donor plate was kept on the acceptor plate like a "sandwich" and incubated at 25 °C for 18 h. UV absorbance was used to access the concentration of test samples in donor and acceptor wells. As described earlier, the absorbance was used to calculate the test compound's effective permeability (P_e).[37]

4.10. *In Silico* ADME Properties. The ADME properties of ligands were determined using the QikProp module of the Schrodinger software. The descriptors and properties for reference ranges are for 95% of known drugs.

■ ASSOCIATED CONTENT

Supporting Information

The Supporting Information is available free of charge at https://pubs.acs.org/doi/10.1021/acsomega.2c07993.

Spectral data scans for all compounds (PDF)

■ AUTHOR INFORMATION

Corresponding Author

Sandip B. Bharate − *Natural Products & Medicinal Chemistry Division, CSIR-Indian Institute of Integrative Medicine, Jammu 180001, India; Academy of Scientific & Innovative Research (AcSIR), Ghaziabad 201002, India;* orcid.org/0000-0001-6081-5787; Phone: +91-191-2586333; Email: sbharate@iiim.res.in, sandipbharate@gmail.com

Author

Ankita Sharma − *Natural Products & Medicinal Chemistry Division, CSIR-Indian Institute of Integrative Medicine, Jammu 180001, India; Academy of Scientific & Innovative Research (AcSIR), Ghaziabad 201002, India*

Complete contact information is available at: https://pubs.acs.org/10.1021/acsomega.2c07993

Author Contributions

S.B.B. designed, executed, and coordinated this study. A.S. synthesized all compounds and performed biological assays and molecular modeling. A.S. and S.B.B. contributed to the manuscript writing.

Notes

The authors declare no competing financial interest.

■ ACKNOWLEDGMENTS

The authors thank the analytical department, IIIM, for analytical support. The financial support from CSIR YSA Grant (P90807) is gratefully acknowledged. IIIM Publication Number. CSIR-IIIM/IPR/00518.

■ ABBREVIATIONS.

AD:Alzheimer's disease; ACh:acetylcholine; ADME:absorption distribution metabolism elimination; BCh:butyrylcholine; BBB:blood−brain barrier; CAS:catalytic anionic site; EeAChE:electric eel cholinesterase; eqBChE:equine serum butyrylcholinesterase; hBACE-1:human amyloid β precursor protein cleaving enzyme or β-secretase; MD:molecular dynamics; NP:natural product; PDB:Protein Data Bank;

PAS:peripheral anionic site; PAMPA:parallel artificial membrane permeability assay; P_e:effective permeability coefficient; RMSD:root mean square deviation; SAR:structure−activity relationship; ThT:thioflavin T

REFERENCES

(1) (a) Tatulian, S. A. Challenges and hopes for Alzheimer's disease. *Drug Discovery Today* **2022**, *27*, 1027−1043. (b) Palmioli, A.; Mazzoni, V.; De Luigi, A.; Bruzzone, C.; Sala, G.; Colombo, L.; Bazzini, C.; Zoia, C. P.; Inserra, M.; Salmona, M.; De Noni, I.; Ferrarese, C.; Diomede, L.; Airoldi, C. Alzheimer's Disease Prevention through Natural Compounds: Cell-Free, In Vitro, and In Vivo Dissection of Hop (*Humulus lupulus* L.) Multitarget Activity. *ACS Chem. Neurosci.* **2022**, *13*, 3152−3167.

(2) Malhotra, P. A. Impairments of attention in Alzheimer's disease. *Curr. Opin. Psychol.* **2019**, *29*, 41−48.

(3) Li, Q.; Yang, H.; Chen, Y.; Sun, H. Recent progress in the identification of selective butyrylcholinesterase inhibitors for Alzheimer's disease. *Eur. J. Med. Chem.* **2017**, *132*, 294−309.

(4) Mehta, M.; Adem, A.; Sabbagh, M. New acetylcholinesterase inhibitors for Alzheimer's disease. *Int. J. Alzheimer's Dis.* **2012**, *2012*, No. 728983.

(5) Swahn, B.-M.; Kolmodin, K.; Karlström, S.; Berg, S.; Söderman, P.; Holenz, J.; Lindström, J.; Sundström, M.; Turek, D.; Kihlström, J.; Slivo, C.; Andersson, L.; Pyring, D.; Rotticci, D.; Ohberg, L.; Kers, A.; Bogar, K.; von Kieseritzky, F.; Bergh, M.; Falting, J.; et al. Design and Synthesis of β-Site Amyloid Precursor Protein Cleaving Enzyme (BACE1) Inhibitors with in Vivo Brain Reduction of β-Amyloid Peptides. *J. Med. Chem.* **2012**, *55*, 9346−9361.

(6) Finder, V. H.; Glockshuber, R. Amyloid-beta aggregation. *Neurodegener. Dis.* **2007**, *4*, 13−27.

(7) Nirmalraj, P. N.; List, J.; Battacharya, S.; Howe, G.; Xu, L.; Thompson, D.; Mayer, M. Complete aggregation pathway of amyloid b (1-40) and (1-42) resolved on an atomically clean interface. *Sci. Adv.* **2020**, *6*, No. eaaz6014.

(8) Vaz, M.; Silva, V.; Monteiro, C.; Silvestre, S. Role of Aducanumab in the Treatment of Alzheimer's Disease: Challenges and Opportunities. *Clin. Interventions Aging* **2022**, *17*, 797−810.

(9) (a) Bharate, S. S.; Mignani, S.; Vishwakarma, R. A. Why Are the Majority of Active Compounds in the CNS Domain Natural Products? A Critical Analysis. *J. Med. Chem.* **2018**, *61*, 10345−10374. (b) Newman, D. J.; Cragg, G. M. Natural Products as Sources of New Drugs from 1981 to 2014. *J. Nat. Prod.* **2016**, *79*, 629−661. (c) Dias, D. A.; Urban, S.; Roessner, U. A historical overview of natural products in drug discovery. *Metabolites* **2012**, *2*, 303−336.

(10) Carneiro, A.; Matos, M.; Uriarte, E.; Santana, L. Trending Topics on Coumarin and Its Derivatives in 2020. *Molecules* **2021**, *26*, No. 501.

(11) (a) Küpeli Akkol, E.; Genç, Y.; Karpuz, B.; Sobarzo-Sánchez, E.; Capasso, R. Coumarins and Coumarin-Related Compounds in Pharmacotherapy of Cancer. *Cancers* **2020**, *12*, No. 1959. (b) Al-Warhi, T.; Sabt, A.; Elkaeed, E. B.; Eldehna, W. M. Recent advancements of coumarin-based anticancer agents: An up-to-date review. *Bioorg. Chem.* **2020**, *103*, No. 104163. (c) Endo, S.; Oguri, H.; Segawa, J.; Kawai, M.; Hu, D.; Xia, S.; Okada, T.; Irie, K.; Fujii, S.; Gouda, H.; Iguchi, K.; Matsukawa, T.; Fujimoto, N.; Nakayama, T.; Toyooka, N.; Matsunaga, T.; Ikari, A. Development of Novel AKR1C3 Inhibitors as New Potential Treatment for Castration-Resistant Prostate Cancer. *J. Med. Chem.* **2020**, *63*, 10396−10411.

(12) (a) Sutar, S. M.; Savanur, H. M.; Malunavar, S. S.; Pawashe, G. M.; Aridoss, G.; Kim, K. M.; Lee, J. Y.; Kalkhambkar, R. G. Synthesis and Molecular Modelling Studies of Coumarin and 1-Aza-Coumarin Linked Miconazole Analogues and Their Antimicrobial Properties. *ChemistrySelect* **2020**, *5*, 1322−1330. (b) Liu, H.; Xia, D. G.; Chu, Z. W.; Hu, R.; Cheng, X.; Lv, X. H. Novel coumarin-thiazolyl ester derivatives as potential DNA gyrase Inhibitors: Design, synthesis, and antibacterial activity. *Bioorg. Chem.* **2020**, *100*, No. 103907.

(13) (a) Pan, Y.; Liu, T.; Wang, X.; Sun, J. Research progress of coumarins and their derivatives in the treatment of diabetes. *J. Enzyme Inhib. Med. Chem.* **2022**, *37*, 616−628. (b) Ranđelović, S.; Bipat, R. A Review of Coumarins and Coumarin-Related Compounds for Their Potential Antidiabetic Effect. *Clin. Med. Insights: Endocrinol. Diabetes* **2021**, *14*, No. 11795514211042023.

(14) (a) Muke, S.; Kaikini, A.; Peshattiwar, V.; Bagle, S.; Dighe, V.; Sathaye, S. Neuroprotective Effect of Coumarin Nasal Formulation: Kindling Model Assessment of Epilepsy. *Front. Pharmacol.* **2018**, *9*, No. 992. (b) Rodríguez-Enríquez, F.; Costas-Lago, M. C.; Besada, P.; Alonso-Pena, M.; Torres-Terán, I.; Viña, D.; Fontenla, J.; Sturlese, M.; Moro, S.; Quezada, E.; Terán, C. Novel coumarin-pyridazine hybrids as selective MAO-B inhibitors for the Parkinson's disease therapy. *Bioorg. Chem.* **2020**, *104*, No. 104203.

(15) Stefanachi, A.; Leonetti, F.; Pisani, L.; Catto, M.; Carotti, A. Coumarin: A Natural, Privileged and Versatile Scaffold for Bioactive Compounds. *Molecules* **2018**, *23*, No. 250.

(16) (a) Mzezewa, S. C.; Omoruyi, S. I.; Zondagh, L. S.; Malan, S. F.; Ekpo, O. E.; Joubert, J. Design, synthesis, and evaluation of 3,7-substituted coumarin derivatives as multifunctional Alzheimer's disease agents. *J. Enzyme Inhib. Med. Chem.* **2021**, *36*, 1606−1620. (b) Singh, A.; Sharma, S.; Arora, S.; Attri, S.; Kaur, P.; Kaur Gulati, H.; Bhagat, K.; Kumar, N.; Singh, H.; Vir Singh, J.; Mohinder Singh Bedi, P. New coumarin-benzotriazole based hybrid molecules as inhibitors of acetylcholinesterase and amyloid aggregation. *Bioorg. Med. Chem. Lett.* **2020**, *30*, No. 127477. (c) Amin, K. M.; Abdel Rahman, D. E.; Abdelrasheed Allam, H.; El-Zoheiry, H. H. Design and synthesis of novel coumarin derivatives as potential acetylcholinesterase inhibitors for Alzheimer's disease. *Bioorg. Chem.* **2021**, *110*, No. 104792. (d) Zhang, J.; Li, J. C.; Song, J. L.; Cheng, Z. Q.; Sun, J. Z.; Jiang, C. S. Synthesis and evaluation of coumarin/1,2,4-oxadiazole hybrids as selective BChE inhibitors with neuroprotective activity. *J. Asian Nat. Prod. Res.* **2019**, *21*, 1090−1103.

(17) (a) Anand, P.; Singh, B.; Singh, N. A review on coumarins as acetylcholinesterase inhibitors for Alzheimer's disease. *Bioorg. Med. Chem.* **2012**, *20*, 1175−1180. (b) Bhatia, R.; Chakrabarti, S. S.; Kaur, U.; Parashar, G.; Banerjee, A.; Rawal, K. R. Multi-Target Directed Ligands (MTDLs): Promising Coumarin Hybrids for Alzheimer's Disease. *Curr. Alzheimer Res.* **2021**, *18*, 802−830.

(18) Sharma, A.; Nuthakki, V. K.; Gairola, S.; Singh, B.; Bharate, S. B. A Coumarin-Donepezil Hybrid as a Blood-Brain Barrier Permeable Dual Cholinesterase Inhibitor: Isolation, Synthetic Modifications, and Biological Evaluation of Natural Coumarins. *ChemMedChem* **2022**, *17*, No. e202200300.

(19) Liu, W.; Wu, L.; Liu, W.; Tian, L.; Chen, H.; Wu, Z.; Wang, N.; Liu, X.; Qiu, J.; Feng, X.; Xu, Z.; Jiang, X.; Zhao, Q. Design, synthesis and biological evaluation of novel coumarin derivatives as multifunctional ligands for the treatment of Alzheimer's disease. *Eur. J. Med. Chem.* **2022**, *242*, No. 114689.

(20) Sharma, M.; Sharma, A.; Nuthakki, V. K.; Bhatt, S.; Nandi, U.; Bharate, S. B. Design, synthesis, and structure-activity relationship of caffeine-based triazoles as dual AChE and BACE-1 inhibitors. *Drug Dev. Res.* **2022**, *83*, 1803−1821.

(21) (a) Najafi, Z.; Mahdavi, M.; Saeedi, M.; Karimpour-Razkenari, E.; Asatouri, R.; Vafadarnejad, F.; Moghadam, F. H.; Khanavi, M.; Sharifzadeh, M.; Akbarzadeh, T. Novel tacrine-1,2,3-triazole hybrids: In vitro, in vivo biological evaluation and docking study of cholinesterase inhibitors. *Eur. J. Med. Chem.* **2017**, *125*, 1200−1212. (b) Le-Nhat-Thuy, G.; Nguyen Thi, N.; Pham-The, H.; Dang Thi, T. A.; Nguyen Thi, H.; Nguyen Thi, T. H.; Nguyen Hoang, S.; Nguyen, T. V. Synthesis and biological evaluation of novel quinazoline-triazole hybrid compounds with potential use in Alzheimer's disease. *Bioorg. Med. Chem. Lett.* **2020**, *30*, No. 127404. (c) Mohammadi-Khanaposhtani, M.; Saeedi, M.; Zafarghandi, N. S.; Mahdavi, M.; Sabourian, R.; Razkenari, E. K.; Alinezhad, H.; Khanavi, M.; Foroumadi, A.; Shafiee, A.; Akbarzadeh, T. Potent acetylcholinesterase inhibitors: design, synthesis, biological evaluation, and docking study of acridone linked to 1,2,3-triazole derivatives. *Eur. J. Med. Chem.* **2015**, *92*, 799−806.

https://doi.org/10.1021/acsomega.2c07993
ACS Omega 2023, 8, 11161−11176

(22) Monceaux, C. J.; Hirata-Fukae, C.; Lam, P. C. H.; Totrov, M. M.; Matsuoka, Y.; Carlier, P. R. Triazole-linked reduced amide isosteres: an approach for the fragment-based drug discovery of anti-Alzheimer's BACE1 inhibitors. *Bioorg. Med. Chem. Lett.* **2011**, *21*, 3992−3996.
(23) Kaur, A.; Narang, S. S.; Kaur, A.; Mann, S.; Priyadarshi, N.; Goyal, B.; Singhal, N. K.; Goyal, D. Multifunctional Mono-Triazole Derivatives Inhibit Aβ42 Aggregation and Cu2+-Mediated Aβ42 Aggregation and Protect Against Aβ42-Induced Cytotoxicity. *Chem. Res. Toxicol.* **2019**, *32*, 1824−1839.
(24) Nuthakki, V. K.; Mudududdla, R.; Sharma, A.; Kumar, A.; Bharate, S. B. Synthesis and biological evaluation of indoloquinoline alkaloid cryptolepine and its bromo-derivative as dual cholinesterase inhibitors. *Bioorg. Chem.* **2019**, *90*, No. 103062.
(25) Raghuvanshi, R.; Jamwal, A.; Nandi, U.; Bharate, S. B. Multitargeted C9-substituted ester and ether derivatives of berberrubine for Alzheimer's disease: Design, synthesis, biological evaluation, metabolic stability, and pharmacokinetics. *Drug Dev. Res.* **2023**, *84*, 121−140.
(26) Hamed, M. Y. Prediction of Drug Potencies of BACE1 Inhibitors: A Molecular Dynamics Simulation and MM_GB(PB)SA Scoring. *Computation* **2020**, *8*, No. 106.
(27) Bharadwaj, P. R.; Dubey, A. K.; Masters, C. L.; Martins, R. N.; Macreadie, I. G. Abeta aggregation and possible implications in Alzheimer's disease pathogenesis. *J. Cell. Mol. Med.* **2009**, *13*, 412−421.
(28) Luhrs, T.; Ritter, C.; Adrian, M.; Riek-Loher, D.; Bohrmann, B.; Dobeli, H.; Schubert, D.; Riek, R. 3D structure of Alzheimer's amyloid-beta(1-42) fibrils. *Proc. Natl. Acad. Sci. U.S.A.* **2005**, *102*, 17342−17347.
(29) Sari, S.; Kaynak, F. B.; Dalkara, S. Synthesis and anticonvulsant screening of 1,2,4-triazole derivatives. *Pharmacol. Rep.* **2018**, *70*, 1116−1123.
(30) Xia, Y.-L.; Wang, J.-J.; Li, S.-Y.; Liu, Y.; Gonzalez, F. J.; Wang, P.; Ge, G.-B. Synthesis and structure-activity relationship of coumarins as potent Mcl-1 inhibitors for cancer treatment. *Bioorg. Med. Chem.* **2021**, *29*, No. 115851.
(31) López-Rojas, P.; Janeczko, M.; Kubiński, K.; Amesty, Á.; Masłyk, M.; Estévez-Braun, A. Synthesis and Antimicrobial Activity of 4-Substituted 1,2,3-Triazole-Coumarin Derivatives. *Molecules* **2018**, *23*, No. 199.
(32) Augustin, N.; Nuthakki, V. K.; Abdullaha, M.; Hassan, Q. P.; Gandhi, S. G.; Bharate, S. B. Discovery of helminthosporin, an anthraquinone isolated from *Rumex abyssinicus* jacq as a dual cholinesterase inhibitor. *ACS Omega* **2020**, *5*, 1616−1624.
(33) Cheung, J.; Rudolph, M. J.; Burshteyn, F.; Cassidy, M. S.; Gary, E. N.; Love, J.; Franklin, M. C.; Height, J. J. Structures of Human Acetylcholinesterase in Complex with Pharmacologically Important Ligands. *J. Med. Chem.* **2012**, *55*, 10282−10286.
(34) Rosenberry, T. L.; Brazzolotto, X.; Macdonald, I. R.; Wandhammer, M.; Trovaslet-Leroy, M.; Darvesh, S.; Nachon, F. Comparison of the Binding of Reversible Inhibitors to Human Butyrylcholinesterase and Acetylcholinesterase: A Crystallographic, Kinetic and Calorimetric Study. *Molecules* **2017**, *22*, No. 2098.
(35) Patel, S.; Vuillard, L.; Cleasby, A.; Murray, C. W.; Yon, J. Apo and inhibitor complex structures of BACE (beta-secretase). *J. Mol. Biol.* **2004**, *343*, 407−416.
(36) Abdullaha, M.; Nuthakki, V. K.; Bharate, S. B. Discovery of methoxy-naphthyl linked N-(1-benzylpiperidine) benzamide as a blood-brain permeable dual inhibitor of acetylcholinesterase and butyrylcholinesterase. *Eur. J. Med. Chem.* **2020**, *207*, No. 112761.
(37) Nuthakki, V. K.; Yadav Bheemanaboina, R. R.; Bharate, S. B. Identification of aplysinopsin as a blood-brain barrier permeable scaffold for anti-cholinesterase and anti-BACE-1 activity. *Bioorg. Chem.* **2021**, *107*, No. 104568.

https://doi.org/10.1021/acsomega.2c07993
ACS Omega 2023, 8, 11161−11176